The effect of breaking-induced turbulence on sediment entrainment in the surfzone

MSc thesis Earth Surface and Water,
Coastal dynamics and River systems

Name: Winnie de Winter (3352110)
Supervisor: Dr. B.G. Ruessink
Second corrector: Dr. F. Grasso
Second version: May 22, 2013

Utrecht University
Department of Physical Geography
Faculty of Geosciences

Contents

1. Introduction

Beaches, together with the foreshore, act as a natural defense against inundation of the inland area during storms. In coastal policy making, it is therefore important to maintain the coast in its protective state, for example by nourishments. Erosion and accretion of the coastal area are determined by sediment transport in the surfzone. So, their prediction is one of the most prominent research subjects for coastal morphologists. In this way it is tried to make a more accurate prediction whether a coast is eroding or accreting and how human interference affects coastal evolution. Sediment can be transported by cross-shore and alongshore processes. In the surfzone, the waves and wave-induced processes are the most prominent factor for sediment suspension and subsequent transport.

In the surf zone, turbulence is generated both by breaking waves and near-bed shear stresses of mean flows in cross-shore and alongshore direction. Under a breaking wave, turbulence is generated in two separate boundary layer regimes, namely the bottom boundary layer (BBL) and the surface boundary layer (SBL) (Feddersen, 2012). The SBL is generated at the water surface due to wave breaking and the BBL is generated due to friction near the bed which causes vortices. In the surfzone, where the water depth is sufficiently shallow, these two boundary layers can overlap (Feddersen, 2012). Here, the surface-generated turbulence, driven by wave breaking, is dominant over the bottom-generated turbulence. However, the effect of the BBL remains important and cannot be neglected (Grasso and Ruessink, 2011). Intermittently, the breaking-induced turbulence reaches the sea bed and stirs up the sediment (Nadoaka et al., 1988).

There is a difference in sediment suspension between the deep water and shallow water regions. In deep water sediment suspension is in phase with the orbital wave motions. Here, sediment is suspended due to BBL turbulence. In shallow water sediment suspension is intermittent and may be related to wave-breaking turbulence (Scott et al., 2009). During these intermittently wave-breaking turbulence events, there is a significant increase in suspended sediment concentrations in the water column (Ogston and Sternberg, 2002) . Principally, in models, sediment transport calculations are described by empirical relations, because the physical processes underlying sediment transport in the surf zone are not well understood. In these relations, transport is only related to the orbital motion of waves. At present, sediment suspension due to wave-breaking turbulence is not taken into account in these models. Actually, when the effect of turbulence on the shear stress is combined with a Bagnold-type model, the calculations for sediment transport are significantly improved (Butt et al., 2004). Breaking wave turbulence could also be an important factor in the mechanism

of bar formation in the nearshore (Roelvink and Stive, 1989), a major subject that is still not well understood. Despite these indications, breaking-induced turbulence and sand transport are not well understood and not part of coastal evolution models.
To improve sediment transport predictions, various approaches are possible. Most previous studies were small-scale laboratory flume experiments (e.g. Nadaoka et al., 1988; Cox and Kobayashi, 2000; Govender et al., 2004), which have problems with scale-effects in sediment transport. The limited number of existing field experiments (e.g. Yu et al., 1993; Beach and Sternberg, 1996; Ogston and Sternberg, 2002; Butt et al., 2004; Aagaard and Hughes, 2010; Ruessink, 2010; Grasso and Ruessink, 2011), have the disadvantage that environmental conditions cannot be controlled and the observed transports are a complicated interplay of numerous processes.

This research report is based on a large-scale, prototype flume experiment and focuses on the effect of wave-breaking turbulence on sediment suspension in the surfzone.
The measurements for this research are carried out at the Delta Flume of Deltares, during the EU-Hydralab IV BARrier Dynamics Experiment (BARDEX II).

This thesis will start with a literature review about breaking-induced turbulence and sediment suspension in the surfzone in chapters 2 and 3, respectively. Then, the aim of the research is defined and the problem definition will be given in chapter 4 followed by research questions drawn up to solve the problems. Hypotheses will be made using the literature review. From here, the experimental setup and data processing are clarified in the methods (chapter 5). Results of the turbulence and sediment suspension problems will be given in chapters 6 and 7, respectively. Thereafter, in chapter 8, the results will be discussed and compared with the results mentioned in the literature review. The conclusions of this research are summarized in chapter 9.

2. Turbulence under breaking waves (literature)

In this section first the generation of turbulence due to breaking waves is elaborated, hereafter it is discussed how the source of turbulence can be determined and finally the occurrence of significant wave-breaking turbulence is discussed. Turbulence can be determined in three different ways: turbulent kinetic energy (k [m^2s^{-2}]), energy dissipation rate (ε [m^2s^{-2}]) or Reynolds stress (u' w' [m^2s^{-2}]). Here, these three terms are used to explain the topics about turbulence.

2.1 Obliquely Descending Eddies (ODE) and the vertical distribution of turbulence in the water column

In almost the entire surf zone area, there is a certain distinctive eddy structure under breaking waves (Nadaoka, 1986). Near the wave crest, parallel to the crest line, the prominent eddies have a two-dimensional flow structure. When the wave crest has passed, the two-dimensional flow structure transforms into a three-dimensional structure which descends into the water column (Nadaoka, 1986; Nadoaka et al., 1988) (Figure 1). These three-dimensional descending eddies are referred to as "obliquely descending eddies" (ODE) (Nadaoka, 1986; Nadoaka et al., 1988). ODE play an important role for the generation of the Reynolds stress and they transport the horizontal flow (when u>0) downward into the water column (when w<0) (Cox and Kobayashi, 2000).

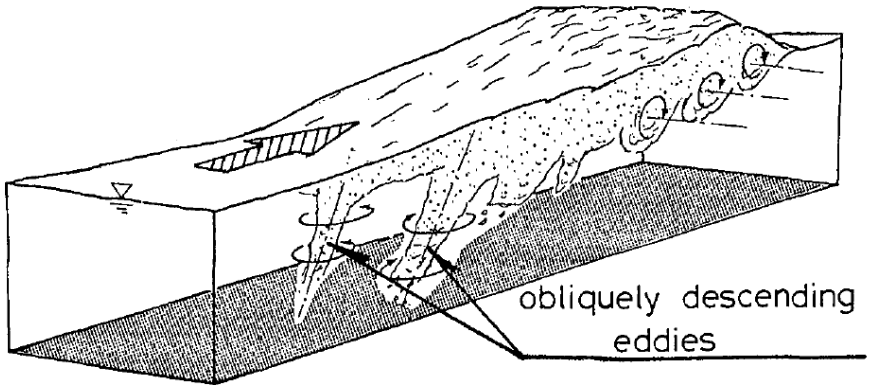

Figure 1: Schematic representation of the two-dimensional and three-dimensional ODE under breaking waves. (Nadaoka, 1986)

Behind the wave crest, where the ODE are formed, the turbulence intensity is almost uniform over the water depth (Nadaoka et al., 1988). This is clearly visible in Figure 2. The arrows indicate an identical location, but different elevations above the bed and thus the ODE. The turbulence intensity measured at the upper most level above the bed is quite large and when the turbulence moves downward into the water column (arrows) the decrease in the turbulence intensity is not notably large. This means that the obliquely descending eddies

bring quite a large turbulence intensity to the sea bed (Nadaoka et al., 1988), which can be an important fact for the entrainment of sediment.

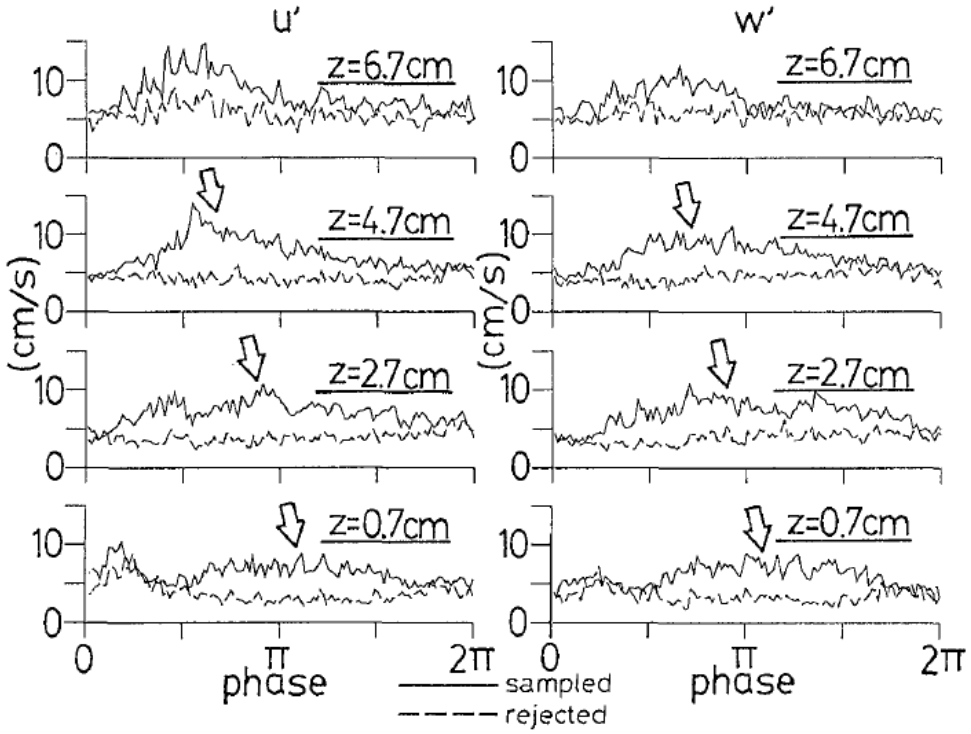

Figure 2: Phase-averaged turbulence intensities u'(cm/s) and w'(cm/s) at different heights above the bed. (Nadaoka et al., 1988)

The vertical variation of the time-averaged turbulent kinetic energy ($\bar{k}$ [cm^2s^{-2}]) depends on the location in the cross-shore profile (Scott et al., 2005). In Figure 3 the variation of $\bar{k}$ in the cross-shore and vertical direction is shown. Waves are breaking over the bar, region P4-P6 in Figure 3, with intensive wave-breaking at P4. In the vertical structure of $\bar{k}$ in these wave breaking regions, it can be seen that $\bar{k}$ is large near the water surface and decays toward the bed level. During wave-breaking, high turbulence intensities are generated near the water surface and decrease towards the sea bed when turbulence penetrates the water column. Thus, an increase in $\bar{k}$ near the water surface indicates the presence of breaking-induced turbulence. It can be noticed that, at location P5 and P6 the $\bar{k}$ approaches zero near the bed, whereas at location P4, the value of $\bar{k}$ is still considerably large near the bed. This is probably due to the intensive wave-breaking at this location, so the ODE can bring high turbulent intensities to the sea bed as noted earlier (Nadaoka et al., 1988).

Turbulence extending to the bed, results in local increases in shear stresses (Aagaard and Hughes, 2010). This indicates that breaking waves at a bar generate turbulence that might be important for near-bed processes, such as the entrainment of sediment in the water

column due to surface generated turbulence. After wave breaking, the turbulence is confined to the upper part of the water column and will be dissipated when waves reform (Scott et al., 2005).

The vertical variation of turbulence in the surfzone can indicate the source of the turbulence in the water column, which is the water surface (wave-breaking) or the sea bed (bottom friction). This will be discussed in the following section.

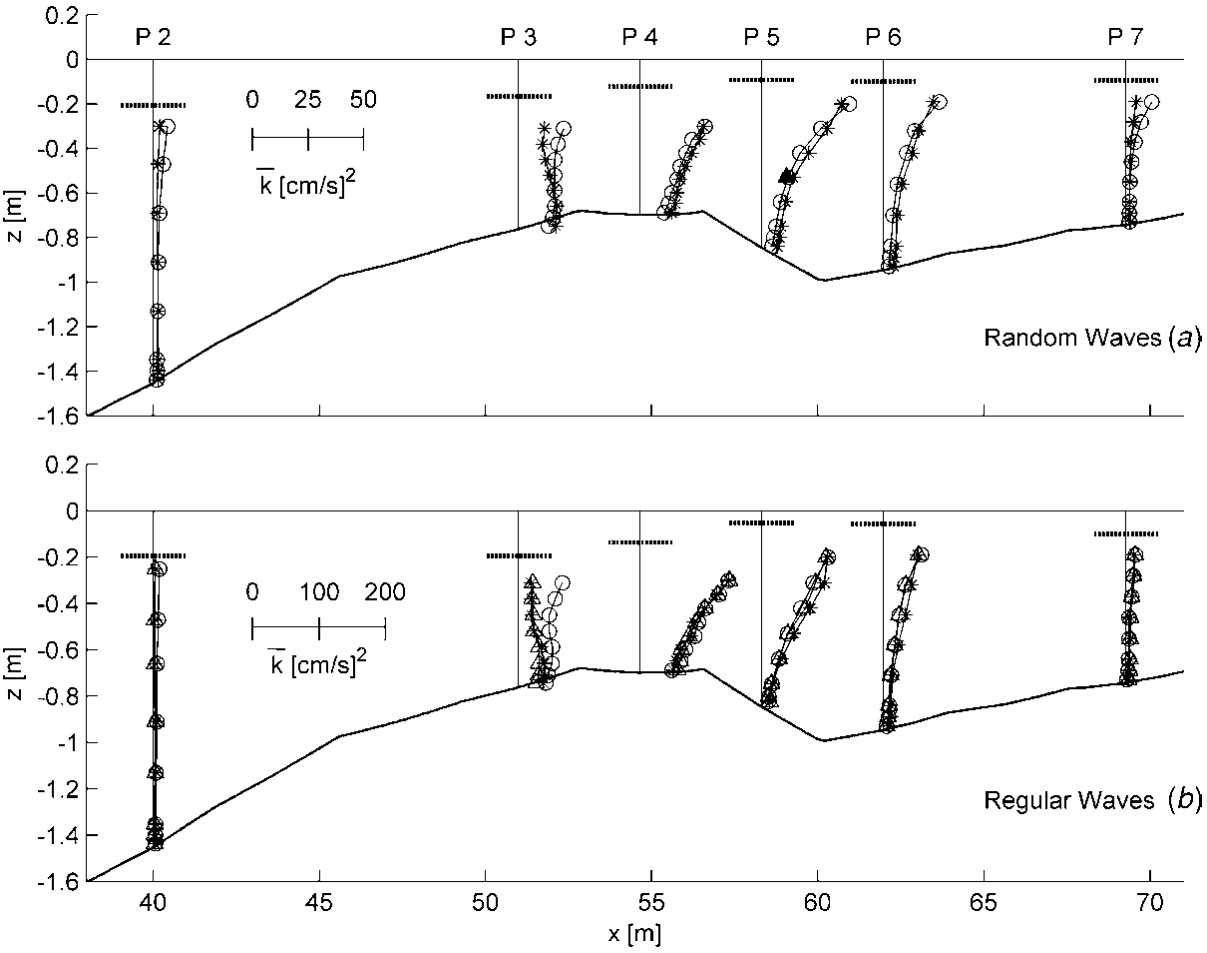

Figure 3: Cross-shore and vertical variation of $\overline{k}$ (cm^{2}s^{-2}) for (a) random and (b) regular waves over a fixed barred beach. (Scott et al., 2005)

2.2 Source of turbulence in the vertical water column

The vertical distribution of the surface-generated relative to the bed-generated turbulence can be displayed in terms of the turbulence dissipation rate ε (m^{2}s^{-2}) (Figure 4). Figure 4 shows the relation between the vertical profile of the measured average dissipation rate and different wave breaking conditions. The values 0.38 and 0.48 for H_s/h indicate approximate boundaries between non-breaking, weakly breaking and fully breaking conditions (Ruessink, 2010). When ε increases near the sea bed, it means that the bed-generated turbulence is

the most important turbulence source and when ε increases near the water surface, the surface-generated turbulence due to breaking waves is the most dominant turbulence source. In relative deep water (Figure 4a), different relative wave heights show different vertical profiles of ε. In the case weakly breaking conditions (pink open circles) there is a strong increase in ε near the sea bed, whilst the increase of ε near the water surface it is not that obvious. This indicates that here the bed-generated turbulence is of larger importance than the surface-generated turbulence. When the relative wave height, and thus the wave-breaking intensities, increase the dissipation rate increases as well and its vertical structure changes. With increasing wave-breaking intensities, there is a large increase in ε near the water surface, whilst near the sea bed ε has not increased that much compared to the central measuring point of the vertical profile. This indicates that the surface-generated turbulence becomes more dominant with increasing wave-breaking intensities. When moving shoreward, at more shallow water depths (Figure 4b-d), the differences in the dissipation rates between weakly and fully wave-breaking conditions are still recognizable. Dissipation rates for weakly wave-breaking conditions are smaller compared to the fully wave-breaking conditions. Also, the difference in the vertical structure remains visible. During the weakly wave-breaking conditions the bed-generated turbulence is still the main source of turbulence, whilst in stronger wave-breaking conditions the importance of the surface-generated turbulence increases.

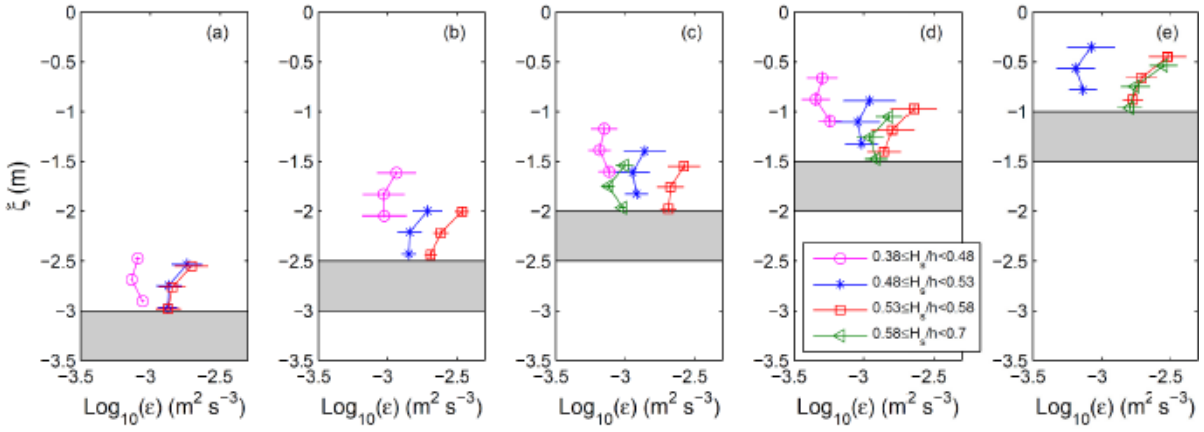

Figure 4: Average dissipation rate measured at three ADVOs at different heights above the bed versus the elevation of the instruments ξ (ξ=z-h). (a) 3≤*h*<3.5 m, (b) 2.5≤*h*<3 m, (c) 2≤*h*<2.5 m, (d) 1.5≤*h*<2 m and (e) 1≤*h*<1.5 m. A small value for H_s/h indicates weakly breaking conditions and a large value indicates fully breaking conditions, values in between indicate moderate breaking conditions. The grey beams represent the locations of the sea bed. (Grasso and Ruessink, 2011)

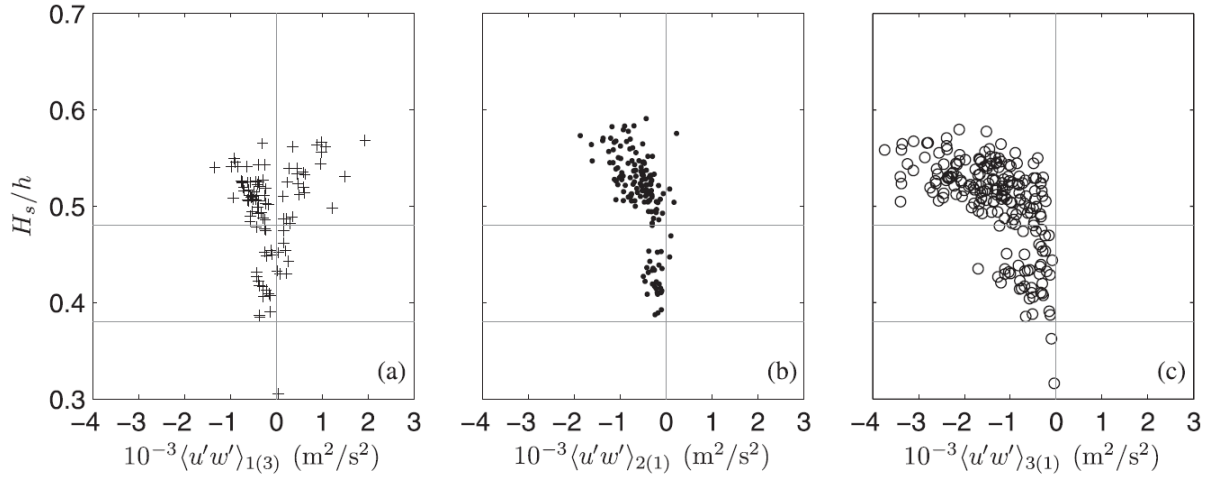

Figure 5: Time-averaged cross-shore Reynolds stress versus relative wave height H_s/h. The two horizontal lines indicate the approximate boundaries between breaking conditions. The line at H_s/h= 0.38 represents the boundary between nonbreaking and weakly breaking waves and the line at H_s/h= 0.48 represents the boundary between weakly breaking and fully breaking conditions. (Ruessink, 2010)

Just like the turbulence dissipation rate, the Reynolds stress (m^2s^{-2}) due to surface-generated turbulence is predominant in the cross-shore direction of the surf zone, compared to the bed-generated Reynolds stress (Figure 5b and 5c). However, in the longshore direction this is the other way around, here bottom boundary layer processes are predominant (Ruessink, 2010). As mentioned earlier, ODE penetrate downward into the water column and generate Reynolds stresses. The motion in downward direction gives negative values for the Reynolds stress. This is why negative values for the time-averaged cross-shore Reynolds stress <u'w'> (m^2s^{-2}) indicate a surface-generated Reynolds stress. So in Figure 5b and 5c the Reynolds stress is mainly negative, implying the existence of surface-generated turbulence. During weak wave-breaking conditions (between the horizontal lines of H_s/h= 0.38 and 0.48) the Reynolds stress is slightly negative and still around 0. This indicates that during weak wave-breaking conditions, less ODEs are generated and thus less turbulence is present. Though, when H_s/h≥0.48 (fully wave-breaking conditions), the Reynolds stress becomes more negative, indicating the presence of a lot of turbulence and high turbulence intensities. However, Figure 5a is in contradiction with Figure 5 b and c. Here, the Reynolds stress apparently can be positive during fully wave-breaking conditions. This may point at the presence of bed generated turbulence. However, it is assumed that the intensity of bed-generated turbulence is an order of magnitude smaller compared to the surface-generated turbulence and thus the positive values in Figure 5a are too large to represent bed-generated turbulence (Ruessink, 2010).

The source of turbulence under breaking waves can also clearly be seen in Figure 3. The vertical structure of the time-averaged turbulent kinetic energy ($\overline{k}$ [cm^2s^{-2}]) is comparable with the vertical structures of turbulence dissipation rate in Figure 4 and of the Reynolds stresses in Figure 5. In Figure 3 at location P4, where intensive wave-breaking is present, there is a strong increase in $\overline{k}$ towards the water surface, which indicates that the source of the turbulence are breaking waves. The fact that $\overline{k}$ does not approach the zero value near the bottom is also an indication that the turbulence is generated by breaking waves (Scott et al., 2005), because this indicates that high turbulence intensities reach the bed. At locations where no wave breaking occurs (P2 and P7) the values of $\overline{k}$ approach zero near the bottom. At location P3 in Figure 3 the maximum value of $\overline{k}$ can be found near the bed. This is probably due to the advection of turbulence in offshore direction coming from location P4 where waves break (Scott et al., 2005).

2.3 The occurrence of wave-breaking turbulence

When wave-breaking turbulence penetrates trough the water column and reaches the sea bed, it can affect the entrainment of sediment (Nadaoka et al., 1988). For this reason the occurrence of wave-breaking turbulence penetrating to the bottom is important. The occurrence of wave-breaking turbulence is intermittent (Nadaoka et al., 1988; Scott et al., 2009) (Figure 6). The occurrence of turbulence near the bottom is indicated with the arrows. A phase difference between the passing of the wave crest and the occurrence of turbulence can be noticed. Turbulence is present at the transition between the wave crest and wave trough passing. Because at this point the orbital wave motion is zero, the intermittent turbulence cannot be caused by the bottom shear stress, but it is generated at the water surface. Another argument is that ODE develop (an increase in the cross-shore velocity u and a decrease in the vertical velocity w) when the wave crest has passed, which is the moment indicated by the arrows.

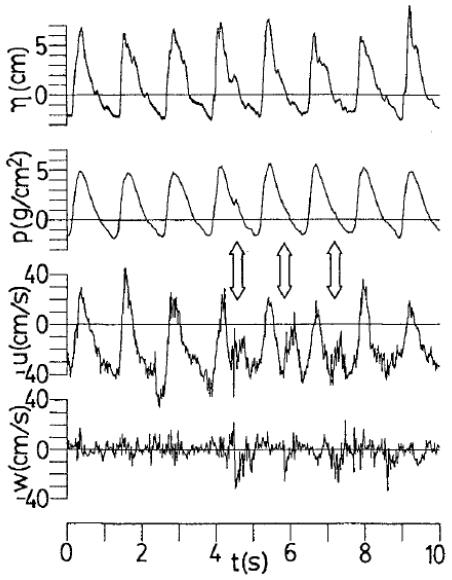

Figure 6: From top to bottom: water surface fluctuation η, bottom pressure fluctuation p and the velocity fluctuations u and w near the sea bed (z = 0.7 cm) in the same time series. (Nadaoka et al., 1988)

The intermittent occurrence of breaking-induced turbulence reaching the bottom, is also clearly visible in Figure 7. The intermittent turbulence in the boundary layer can be recognized at t/T = 22.5 in Figures 7b and 7c. The turbulence event at t/T = 22.5 combined with high increases in the absolute Reynolds shear stress $|\tau|$ (cm^2s^{-2}) and the instantaneous turbulent kinetic energy k (cm^2s^{-2}) indicate that the coherent motion in the bottom boundary layer is caused by wave-breaking turbulence but the occurrence is infrequent (Cox and Kobayashi, 2000).

There is a dependency on wave breaker type whether the turbulence is intense enough or not to reach the sea bed (Aagaard and Hughes, 2010). Figure 8 shows the difference of turbulence between plunging breakers, spilling breakers and shoaling waves. The fourth quadrant of the scatter plots represent the turbulence due to the ODE, since they are determined by a positive cross-shore velocity ($u>0$) and a downward directed vertical velocity ($w<0$) (Cox and Kobayashi, 2000). In the case with plunging breakers (burst 7), there is a cloud of scatter points in the fourth quadrant, indicating the turbulence. In the case with spilling breakers (burst 61) this cloud becomes narrower and is squeezed towards the zero value of the vertical velocity. However, turbulence is still present but it is less intensive due to smaller vertical velocities and probably penetrates less deep into the water column, relative to the turbulence generated by plunging breakers. In the last case with non-breaking shoaling waves (burst 105) the vertical velocity becomes almost zero and the velocity variation remains limited in the cross-shore direction, indicating the presence of orbital wave-motions.

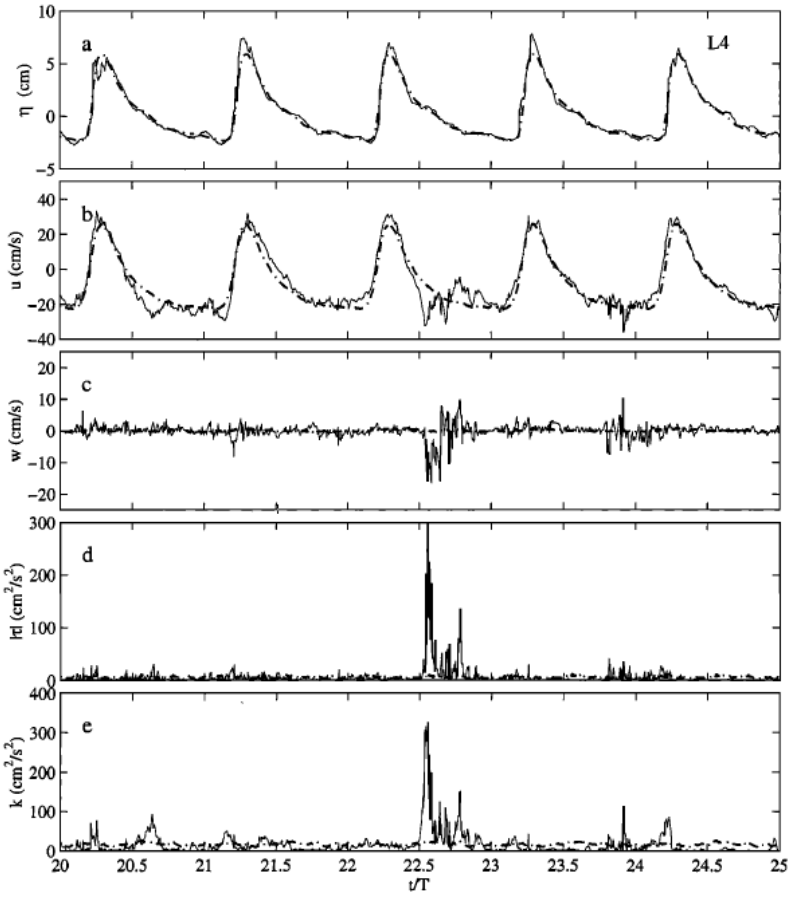

Figure 7: Variation over time of (a) water surface elevation η, (b) cross-shore velocity component u, (c) vertical velocity component w, (d) absolute Reynolds shear stress |τ| and (e) instantaneous turbulent kinetic energy per unit mass k at z = 0.30 cm. All dash-dotted lines are phase-averaged quantities. (Cox and Kobayashi, 2000)

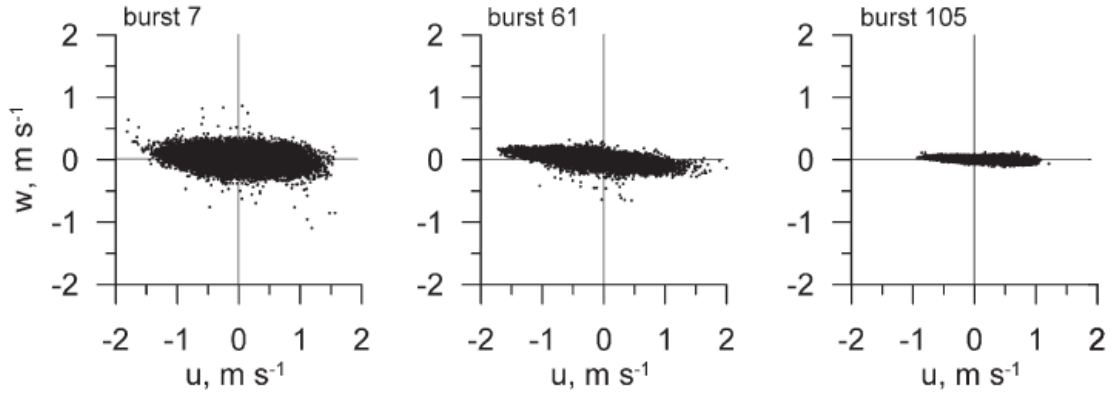

Figure 8: Quadrant scatter plots of instantaneous cross-shore (u) and vertical (w) flow velocities under plunging breakers (burst 7), surf bores (burst 61) and non-breaking shoaling waves (burst 105). (Aagaard and Hughes, 2010)

3. Suspended-sediment transport due to wave breaking turbulence (literature)

As noted earlier, the nature of sediment suspension in shallow water conditions (surfzone) differs from sediment suspension in deep water conditions. In deep water sediment is suspended due to bottom boundary-layer processes and is in phase with the orbital wave motions. In the surfzone, sediment suspension has an intermittent occurrence (Scott et al., 2009), suggesting that it is related to breaking-induced turbulence. The increase in suspended sediment concentrations induced by breaking waves can be large (Ogston and Sternberg, 2002).

In this section first the effect of turbulence on the suspended-sediment concentration is discussed, thereafter the dependency of breaker type on sediment suspension is elaborated and finally it is discussed what the consequences for the prediction of sediment transport are if the wave-breaking turbulence would be taken into account.

3.1 Turbulence and suspended-sediment concentration

Suspended sediment concentration profiles for unbroken waves and broken waves show considerable differences (Figure 9). In the case of unbroken waves (Figure 9a) the maximum sediment concentrations are in a range of 6 to 90 g/l at an elevation less than 1.0 cm above the bed. In the case with broken waves (Figure 9b) this range is much larger, namely >80 g/l at 1.0 cm above the bed. There is also a difference in the upper water column. Under non-breaking waves, the suspended sediment concentrations approach the value of zero in this region, whilst the breaking waves cause sediment concentrations in the range of 0.3 – 1.0 g/l and is typically uniform over depth in the upper water column (Ogston and Sternberg, 2002). From these two observations it can be concluded that breaking waves cause a larger amount of suspended sediment concentrations and the sediment is stirred up higher into the water column compared to sediment suspension due to non-breaking waves. So, breaking-induced turbulence enhances the vertical mixing of suspended sediment in the water column.

Surface generated turbulence at the wave crest causes an upward sediment flux in the water column and thus increases the sediment concentration at wave crests (Aagaard and Hughes, 2010) (Figure 10). The upper panel of Figure 10 shows the variation in the cross-shore and vertical velocities. At t≈965 s, an event of large coherent velocity motions can be recognized, indicating the presence of wave-breaking generated turbulence by plunging breakers. The event starts with a landward directed cross-shore velocity ($u>0$) and a downward vertical velocity ($w<0$). Thereafter the vertical velocity becomes positive ($w>0$) and the cross-shore velocity becomes directed in seaward direction ($u<0$). During this event

suspended sediment concentrations vary within the large range of less than 5 kg/m^3 up to100 kg/m^3. So it can be stated that, the cross-shore sediment flux is very large during wave-breaking turbulence events (Aagaard and Hughes, 2010). Another large peak in the suspended sediment concentration can be seen around t≈972 s. Here, no turbulence event is visible, so this suspension cloud is probably an advected cloud which passed the instruments with a broken wave just seaward of the instruments. The sediment cloud first moved landward, then moved seaward and passed the OBSs (Optical Backscatter Sensors) (Aagaard and Hughes, 2010). It might also be advection by the undertow of a broken wave landward of the instruments.

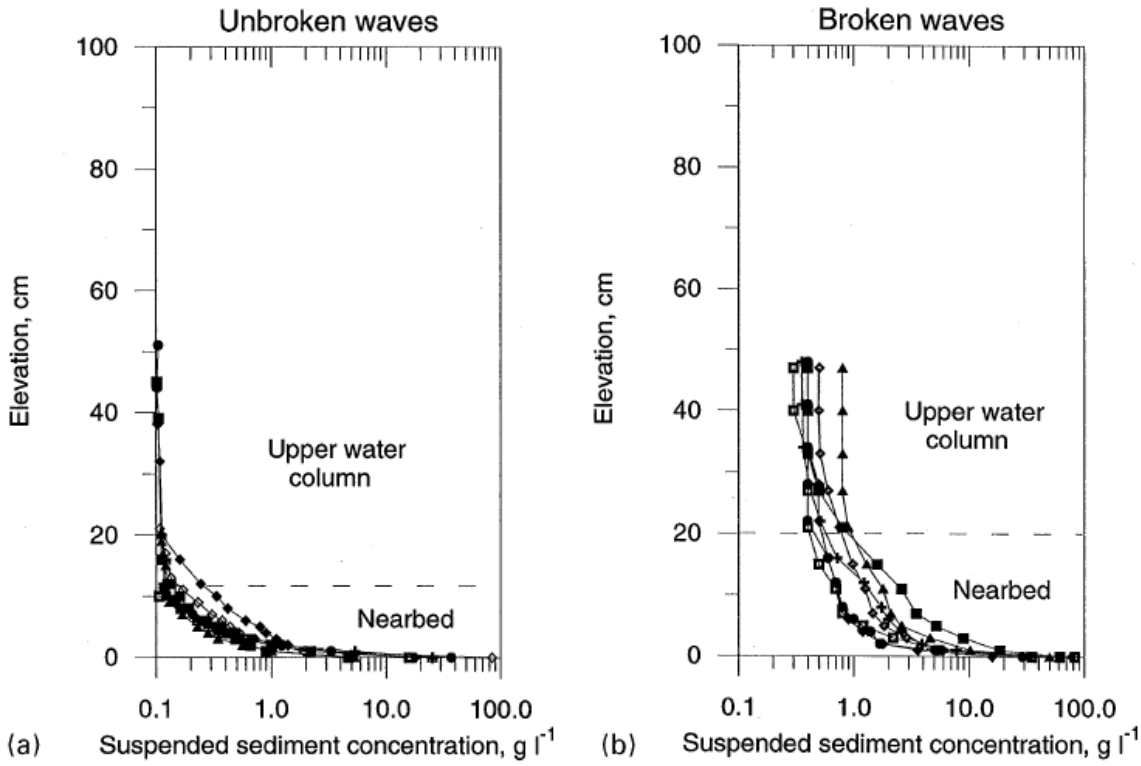

Figure 9: Time-averaged suspended-sediment concentration for (a) unbroken waves, and (b) broken waves. The dashed line in both panels represents the approximate location of the top of the nearbed region. (Ogston and Sternberg, 2002)

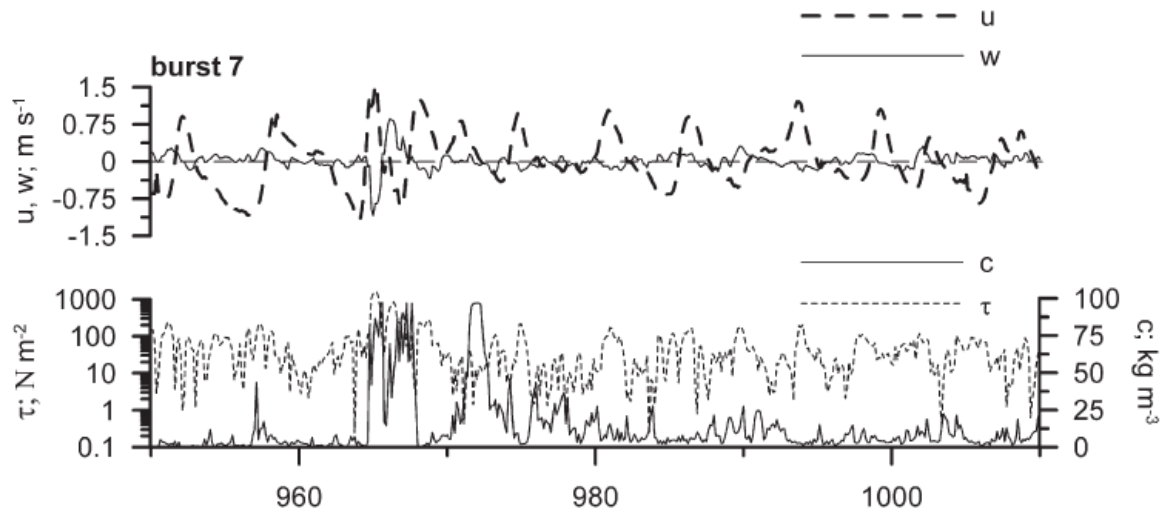

Figure 10: Plunging breakers time series of the cross-shore (u; dashed line) and vertical (w; solid line) velocities (upper panel) and the absolute bed shear stress (|τ|; dotted line) and the near-bed sediment concentration (c; solid line) (lower panel). The x-axis represents time in seconds. (Aagaard and Hughes, 2010)

There is a delay in time between the moment when the waves break and the moment with the maximum suspended-sediment concentration. The timing of the maximum suspended-sediment concentration follows shortly after the waves break (Kana, 1979). This is visible in Figure 10 as well, although this is a very short delay of about 1 second or less. First there is a negative peak of the vertical velocity w at the initiation of the turbulence event and less than a second later the maximum suspended sediment concentration is reached.

Aforementioned, wave breaking causes the occurrence of intermittent wave breaking turbulence, and therefore the increase in sediment suspension is intermittent as well. However, the measured increase of sediment suspension is not always locally generated. The advection of sediment suspension from adjacent areas causes an increase in suspended sediment as well (Scott et al., 2009).

3.2 Sediment suspension and breaker type

The breaker type influences the suspended sediment in the water column under breaking waves (Kana, 1979). The efficiency of sediment suspension is larger under plunging breakers than under surf bores (Aagaard and Hughes, 2010) (Figure 11). In the previous section it was already noticed that during an event of coherent velocity motions under plunging breakers (burst 7) maximum suspended sediment concentrations near the bed could increase up to 100 kg/m^3. In the case with surf bores (burst 61; Figure 11) the maximum suspended sediment concentrations are a factor of 2-3 smaller and they are not clearly related to the pattern in the cross-shore and vertical velocities (Aagaard and Hughes,

2010). Around t≈900 s a small coherent turbulent event can be distinguished. However, there is no clear relation with an increase in suspended sediment concentration. This might be due to the fact that the turbulence generated by this coherent velocity event did not fully penetrate into the water column, reached the bed and stir up sediment. In the case of shoaling waves (burst 105; Figure 11) no coherent turbulent event can be distinguished. There are some minor peaks in the near bed sediment concentrations, but they are related to orbital wave motions during passages of the wave crest or maybe upward mixing of sediment due to bedforms (Aagaard and Hughes, 2010). In Figure 11, burst 105, there is no clear relation visible between the passage of the wave crest and an increase in sediment concentration. However, the absolute bed shear stress does increase during the passage of a wave crest. Under the passage of a wave trough at t≈1862 s, the only significant sediment suspension event occurs. Therefore, it is more likely that the minor peaks are caused by vortex shedding due to bed forms, which enhances the upward mixing of sediment.

The difference in the efficiency of sediment suspension due to different breaker types is because of the difference in the increase of the local bed shear stress, due to extending turbulence to the sea bed. The local bed shear stress is several orders of magnitudes larger under plunging breakers than under surf bores (Aagaard and Hughes, 2010). From this it can be concluded that the breaker type is an important factor in the determination of sediment transport under breaking waves and it might be important to include this in quantitative models which simulate surf zone sediment transport and morphodynamics.

So, plunging waves suspend more sediment, in both the longshore and cross-shore direction, relative to bores, spilling waves and unbroken waves (Beach and Sternberg, 1996). These breaker types show also a difference in the vertical variation of suspended sediment concentrations in the water column. In Figure 12 the vertical suspended sediment distribution at 4 different locations in the surf zone is shown. Location 4 is the most seaward location and location 1 is the most landward location of the surf zone. For plunging breakers a distinction is made between the situation where the instruments are located beneath the foam of breaking waves and the situation where the instruments are situated seaward of the breaking waves (Beach and Sternberg, 1996). At position 4 (Figure 12b) it can be seen that there is a large difference in sediment concentration between the location of breaking waves and the location seaward of the breaking waves. Sediment concentrations under breaking waves are almost twice as large as the sediment concentrations seaward of the breaking waves. However, the nearbed sediment concentrations are equal to each other. The concentration profiles of suspended sediment at the location seaward of the breaking waves are similar to the suspended sediment profiles related to unbroken waves. The only difference is that in the case of unbroken waves there is no rapid increase in sediment concentration near the bed (Beach and Sternberg, 1996).

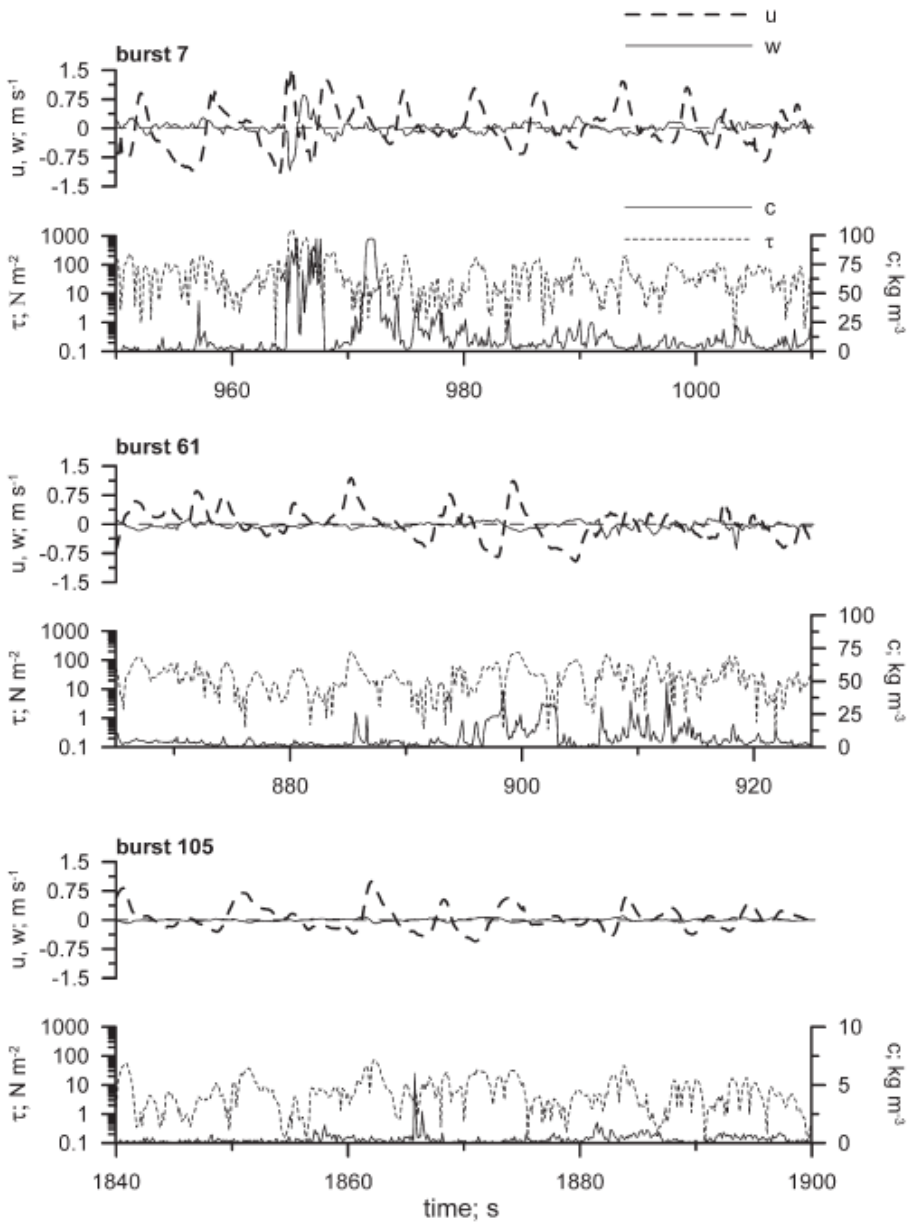

Figure 11: Time series of cross-shore (u; dashed line) and vertical (w; solid line) velocities (every upper panel) and absolute bed shear stress (|τ|; dotted line) and near-bed sediment concentration at z= 0.05 m (c; solid line) (every lower panel). From top to bottom this was obtained under plunging breakers (burst 7), surf bores (burst 61) and non-breaking waves (burst 105). The sediment concentration has different scales in the plots. (Aagaard and Hughes, 2010)

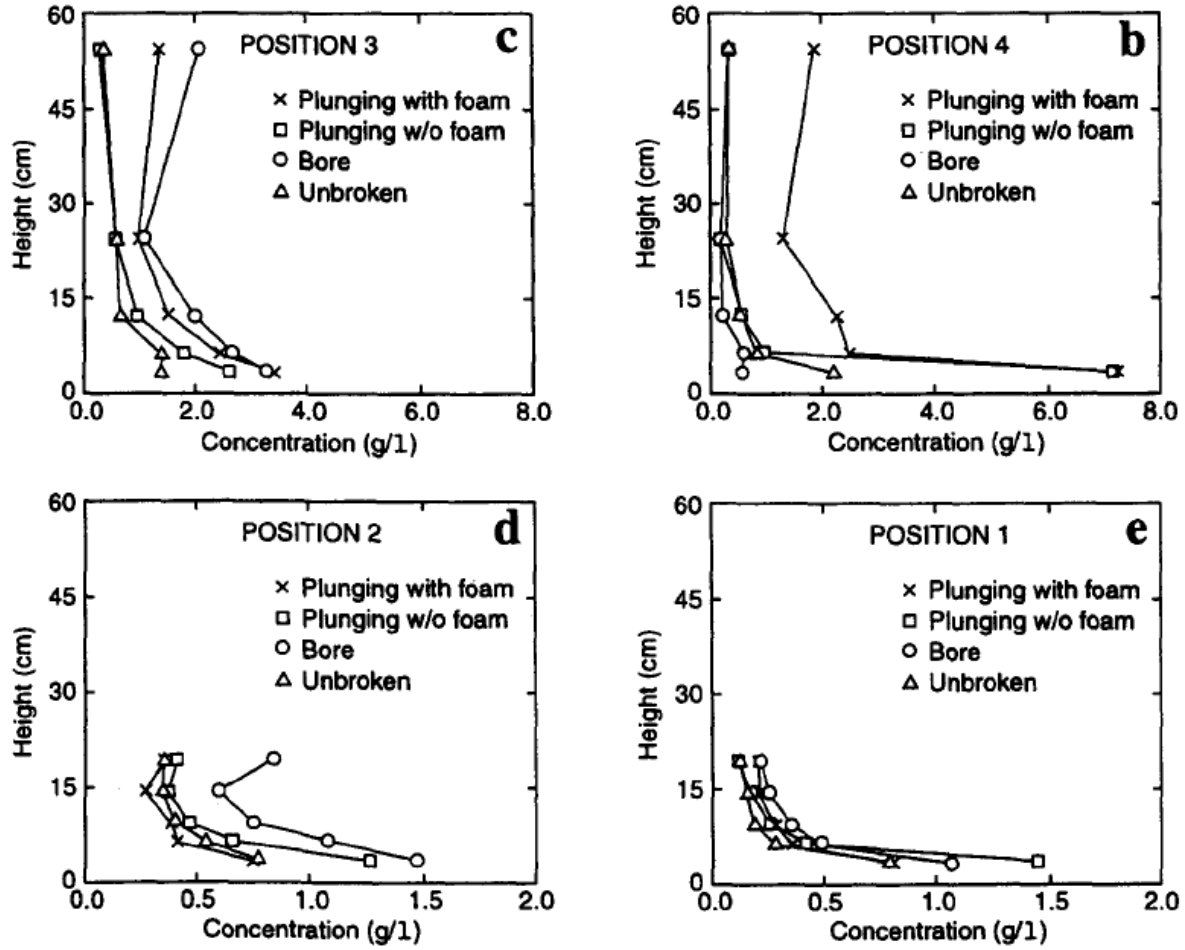

Figure 12: Suspended-sediment distribution across the surf zone as a function of wave type: (b) position 4 (most seaward position), (c) position 3, (d) position 2, and (e) position 1 (most landward position). (Beach and Sternberg, 1996)

3.3 Relation between turbulence and sediment suspension events

Above, it was shown that breaking-induced turbulence can enhance the suspended sediment concentrations in the water column. However, not every high peak in suspended sediment concentration can be related to a turbulence event. Statistics point out that during accretive conditions 37% of the high concentration peaks can be related to locally generated wave-breaking turbulence. In erosive cases this percentage is 22% (Scott et al., 2009). From this it is suggested that for the larger part sediment transport is determined by non-local processes under steep and breaking waves. These non-local processes might be advection of breaking-induced turbulence and sediment suspension events from upstream areas or offshore sediment transport by undertow from broken waves landward of the measuring instruments.

4. Main objectives and research questions

4.1 Summary of the main objectives

In the surfzone, turbulence is generated both at the water surface and near the sea bed. The source of turbulence in the water column can be determined using a vertical turbulence profile. Increasing turbulence at the top of the turbulence profiles point at an increasing importance of surface-generated turbulence induced by breaking waves. Contrary, increasing turbulence at the bottom of the turbulence profile shows an increasing importance of turbulence generated in the bottom boundary layer.

Breaking-induced turbulence is a very important source of turbulence in the surfzone. Increasing wave-breaking conditions result in an increasing dominance of the surface-generated turbulence (Grasso and Ruessink, 2011). High turbulence intensities may penetrate downward into the water column and reach the sea bed. This will stir up the sediment of the sea bed, which is then brought into suspension. Breaking-induced turbulence causes larger suspended sediment concentrations in the water column and the sediment stirs up higher in the water column compared to sediment-suspension under non-breaking waves. The timing of the maximum suspended-sediment concentration follows shortly after the waves break. Not all peak events in suspended sediment concentration can be related to a local turbulence event. Therefore other non-local mechanisms (advection from upstream or sediment transport with undertow) may induce high sediment concentrations near measuring instruments.

Despite a lot of research about breaking-induced turbulence and sediment-suspension, there is still some work to do. This subject is mainly studied during small-scale laboratory flume experiments and in the field. Laboratory experiments have the advantage that the conditions are well-controlled, such that any scenario can be imitated. However, the trouble with the small-scale flume experiments is that sediment transport problems are difficult to approach, because of the scale-effects of sediment. Field experiments do not have the problems with sediment scaling, but the environmental conditions, such as wave conditions or bed morphology, cannot be controlled. For these reasons, experiments at almost prototype scale are suggested. There are some large-scale experiments carried out by Scott et al. (2005) and Yoon and Cox (2010), but Scott et al. (2005) had a fixed sea bed and also Yoon and Cox (2010) did not make observations of sediment-suspension.

4.2 Research questions

As aforementioned, it is important to investigate the sediment transport due to wave-breaking turbulence in more detail on a prototype scale. The definition of the problem is: *What is the effect of wave-breaking induced turbulence on the entrainment of sediment in the surf zone?* The main aim of the research is to examine the effect of wave-breaking induced turbulence on sediment suspension in the surf zone.

The research questions are subdivided into two subsequent topics, wave-breaking-induced turbulence and the following sediment suspension. First, the turbulent part needs to be resolved (question 1). Thereafter, the turbulence knowledge can be used to solve the sediment transport part (question 2).

The first step is to examine the vertical structure of turbulence in the water column. In this way the relevance of breaking-induced to total turbulence can be established. This leads to:

(1a) What is the vertical turbulence structure in the water column under breaking waves?

(1b) Is the turbulence in the water column generated at the sea bed or at the water surface (breaking-induced)?

When the source of the turbulence in the water column is found, it is important to know if surface-generated turbulence is significant to reach the sea bed and affect sand transport.

(2a) When does the surface generated turbulence reach the bed?

(2b) Is there a relation between the occurrence of surface generated turbulence reaching the sea bed and the suspension of sediment?

5. Methods

5.1 Experimental setup

The collection of data was carried out during the EU-Hydralab IV BARrier Dynamics Experiment II (BARDEX II) in the Deltaflume of Deltares, De Voorst, The Netherlands from the 7th of June to the 4th of July 2012. The Deltaflume is a large flume (length = 240 m, width = 5 m and depth = 7m) where experiments of almost prototype scale can be carried out. This is of large importance in this thesis, since the scale-effects of sediment are now absent.

5.1.1 Initial beach profile and measuring equipment

The initial beach profile with a slope of 1:15 (Figure 13) was constructed with medium-sized sand (D_{50} = 0.42 mm, D_{10} = 0.26 mm and D_{90} = 0.90 mm). Pressure transducers (PTs) (Figure 14a) were installed along the cross-shore profile with intervals of about 2.5 m to measure the water surface elevation. Many PTs were positioned close to the flume wall, but some PTs were attached to instrument rigs. Three measuring instrument rigs were positioned on the sloping face of the beach, called miniframe 14 (MF14 located at 59.944 m), miniframe 15 (MF15 located at 70.004 m) and miniframe 16 (MF16 located at 74.852 m). The rigs contained an electromagnetic flow meter (EMF) (Figure 14b) to measure cross-shore flow, three optical backscatter sensors (OBSs) (Figure 14b) at different heights above the bed (0.035 m, 0.070m, and 0.11m) for suspended sediment concentration measurements, and a PT to measure water surface elevations. An additional measuring instrument rig (called CRD) was positioned on the sloping beach face at 64.952 m. The rig was specialized for measuring turbulence and related sediment suspension. This rig contained a PT, three acoustic Doppler velocimeters (ADVs) (Figure 14c) at different heights above the bed (0.175m, 0.435m, and 0.700m) to measure velocities in three dimensions, which can be used to estimate the turbulent velocities. At this rig, ADV1 is the lowest ADV, ADV3 is the upper ADV and ADV2 was positioned in the center of ADV1 and ADV3. During the first wave intervals, it was observed that ADV1 was not working properly, so another ADV was substituted. This caused a difference in the sampling frequency; ADV1 was measuring at 16 Hz and ADV2 and ADV3 were measuring at 10 Hz. Seven OBSs were installed at the CRD rig at different heights above the bed (0.040 m, 0.071 m, 0.104 m, 0.135 m, 0.167 m, 0.440 m, and 0.710 m). Their sampling frequency was 4 Hz. The instruments of all rigs were positioned almost at the centre of the flume, about 2 meter from the flume wall. The vertical position of all four measuring instrument rigs was adjustable. In this way the instruments resumed their initial elevation above the bed at the start of each wave run. A sonar 3D scanner (Figure 14d) was located near the turbulence measuring rig, to receive a three-dimensional scan of the bedform patterns.

After each wave interval, the cross-shore profile was measured at the centre of the flume with a wheel on a carriage rolling over the sea bed.

5.1.2 Hydrodynamic conditions

A wave-paddle at the seaside of the flume created random waves of a JONSWAP spectrum prescribed with a certain significant wave height (H_s) and peak wave period (T_p). H_s, T_p and the water depth (h) were adjusted before the start of every individual wave run during the experiment (Table 1). The number of wave runs and their duration in every serie are listed in Table 1 as well. With these various conditions, turbulence and sediment concentrations were measured at different positions along the cross-shore direction, seaward of the surfzone, at the edge of the surfzone and landward of the edge of the surfzone.

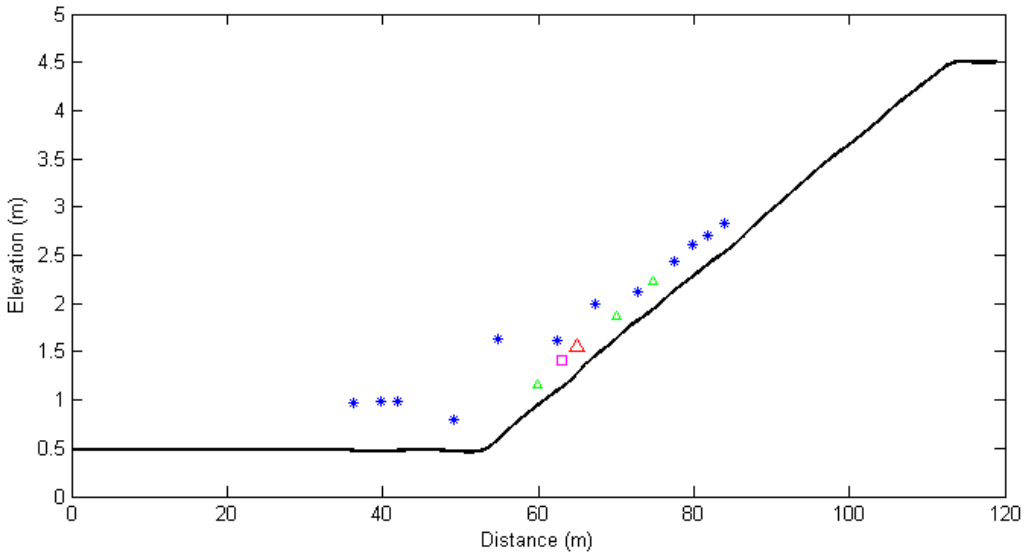

Figure 13: Schematic representation of the experimental setup in cross-shore direction. The blue stars represent the positions of the PTs. MF14, MF15 and MF16 with PTs, EMFs, and OBSs (green triangles) are positioned in the surfzone. The CRD instrument rig (red triangle) with ADVs, OBSs, and a PT was installed to measure turbulence and related sediment suspension. The initial beach profile (black line) has a slope of 1:15.

(a)  (b) 

(c)  (d) 

Figure 14: Measuring instruments. (a) pressure transducer (PT), (b) right: electromagnetic flow meter (EMF) and left: optical backscatter sensors (OBS), (c) acoustic Doppler velocimeters (ADV), and (d) sonar 3D scanner. *Pictures: Daan Wesselman*.

Table 1: Overview of the significant wave height (H_s), peak wave period (T_p) and water depth near the wave paddle (h) during the experiment.

Wave series	H_s (m)	T_p (s)	h (m)	# and duration (minutes) of wave runs
A1	0.8	8	3	3 10 2 15 8 30
A2	0.8	8	3	4 30 1 60
A3	0.8	8	3	1 180 1 15
A4	0.8	8	3	4 30 1 60
A6	0.8	12	3	4 30 1 60
A7	0.6	12	3	4 30 1 60
A8	0.6	12	3	4 30 1 60
B1	0.8	8	3	1 15 3 30 1 60
B2	0.8	8	2.5	4 30 2 60
C1	0.8 and 0.6	8	2.25 → 3.65	11 30
C2	0.6 and 0.8	8	3.53 → 2.25	9 30
D1	0.8	4	3.15 → 4.2	8 20
D2	0.8	5	3.45 → 4.05	5 20
D3	0.8	6	3.45 → 3.9	4 20
D4	0.8	7	3.45 → 3.9	4 20
D5	0.8	8	3.45 → 3.75	3 20
D6	0.8	9	3.30 → 3.75	4 20
D7	0.8	10	3.15 → 3.6	4 20
E1	0.8	8	3.9	5 13

5.2 Data processing

The original dataset contained both data of wave action and periods of no wave action. Therefore the intervals of wave motion were cut out of the data, so the wave data are easy in use. To cancel the effect of the start and end effects of the wave paddle in the flume, the first 40 seconds and the last 20 seconds of every run with wave motion were deleted from the interval.

Raw PT signals were stored in mV. These signals were calibrated to mBar using the individual calibration curves of the PTs and were corrected for atmospheric pressure, which

was measured during the entire experiment. Then the pressure data was translated to water levels using:

$$h = \frac{100p}{\rho g} \quad [1]$$

where h is the water level (m), p is the calibrated pressure (mBar), ρ is the water density ($1000\ kg/m^3$) and g is the acceleration of gravity ($9.81\ m/s^2$). The factor 100 transforms the pressure in mBar into the unit Pa.

The use of water pressure combined with the bed profiles and the vertical position of the measuring instruments, the sea surface elevation (η) was computed. Using η and linear wave theory, a Power Spectral Density (PSD) diagram was computed for each wave run. The Hamming window block length was set to 4.5 minutes with an overlap of 50%. The high frequency range for short waves was set to 0.05 – 2 Hz. From this PSD diagram the short-wave significant wave height (H_s) was derived.

Raw EMF signals were stored in mV. These signals were calibrated to velocities (m/s) using the individual calibration curves of the EMFs. The EMF data of the cross-shore u (m/s) and alongshore v (m/s) velocities were despiked with the Phase-Space Thresholding method (PST) (Mori et al., 2007). Here, the λ used in the Mori method, is multiplied by a factor of 2 to eliminate excessive despiking during the measurements of asymmetric waves: $\lambda = 2 * \sqrt{2 * n}$. This factor was determined by trial and error. The EMFs were rotated such that the wave-angle is 0, because the generated waves had an perpendicular incident wave angle relative to the shoreline.

A quality control (Elgar et al., 2005) was executed to the raw ADV velocity data to reject inaccurate data collected during the passage of a wave trough, bubbles or suspended sediment in front of the sensor. For ADV1 (Nortek) the threshold amplitude for the backscattered signal was set to 5, so signal amplitudes smaller than 5 were rejected. For ADV2 and ADV3 (Sontek) the threshold amplitude for the backscattered signal was set to 100. The ADV data of the cross-shore u (m/s), alongshore v (m/s) and vertical w (m/s) velocities were despiked in two steps using the critical correlation of Elgar et al., 2005 and the Phase-Space Thresholding method of Mori et al., 2007. The critical correlation is determined by $0.3 + 0.4\sqrt{Fs/25} * 100$, where Fs is the sampling frequency (Hz). Thus, for ADV1 (Fs = 16 Hz) the critical correlation is 62% and for ADV2 and ADV3 (Fs = 10 Hz) this is 55%. Velocities with a smaller correlation were rejected. Here λ, used for the Phase-Space method, was multiplied by a factor of 1.7. The ADVs were rotated in the horizontal plane (“u,v” -plane), such that the averaged incident wave-angle is again 0. The orientation

of the probes was as follows. Velocities in cross-shore direction (u) are positive in landward direction, vertical velocities (w) are positive in upward direction. Velocities in alongshore direction (v) cannot be negative caused by the use of a different kind of coordinate system. Because ADV1 was sampling at a higher frequency than ADV2 and ADV3, ADV1 was re-sampled to 10 Hz for later data analysis.

Data of the OBSs were adjusted when the measured value in mV was smaller than 5 during intervals of still water. These low values may point to burial of the OBSs in the sand bed or exposure to huge bubble loads or even above the water level. Sand concentrations were obtained using the calibration curve determined with sand from the flume at the related cross-shore positions of the instruments. To remove the offsets from the data a spline was subtracted from the data, which was determined by 3-minute block minimum values.

The bed profiles measured after every wave interval were smoothed to cancel the influence of ripples on the estimation of water depths. This was done using the quadratic loess filter with lx = 3.5 m (Schlax and Chelton, 1992). This factor removes the ripples but larger-scale features, such as bars that developed during the experiments can still be recognized.

5.3 Data analysis

5.3.1 Turbulent kinetic energy

The observed velocities (u, v and w) in the nearshore consist of three components. Here, an example for the equation of the cross-shore velocity u (m/s) is given:

$$u = \bar{u} + \tilde{u} + u' \qquad [2]$$

where the overbar signifies the time-averaged (mean) velocity, the tilde signifies velocities induced by the motion of waves and the prime signifies the turbulent velocity.

The calculations of the time-averaged turbulent kinetic energy per unit mass ($\bar{k}$ (m^2s^{-2})) and the instantaneous turbulent kinetic energy (k (m^2s^{-2})) require the cross-shore (u'(m/s)), alongshore (v' (m/s)) and vertical (w' (m/s)) turbulent velocities:

Time-averaged turbulent kinetic energy per unit mass

$$\bar{k} = \frac{1}{2}\left(\overline{u'^2} + \overline{v'^2} + \overline{w'^2}\right) \qquad [3]$$

Instantaneous turbulent kinetic energy

$$k = \frac{1}{2}\left(u'^2 + v'^2 + w'^2\right) \qquad [4]$$

To separate the wave-induced velocities and the turbulent velocities, several methods have been developed. However, this remains a quite complicated issue. Here, the Feddersen and Williams (2007) method is used. Using this method, the linear filtering is applied to the ADV velocity measurements followed by the Trowbridge (1998) differencing method. The

Feddersen and Williams (2007) method gives an estimation of the turbulent velocities using two adjacent ADV sensors. Coherent motions between the two sensors are determined as wave motions. The difference between the orbital wave velocities of the two adjacent sensors is identified as a non-coherent motion and thus the turbulence components. This estimation is executed separately for velocities in all three dimensions (u, v and w). In this report subscripts will indicate which ADV sensor is used to estimate the turbulence at the height of a certain ADV sensor. For example, $\bar{k}_{1(2)}$denotes the time-averaged turbulent kinetic energy per unit mass at the height of ADV sensor 1, estimated with ADV sensor 2. Since 3 ADVs were measuring, the turbulent velocities at a certain ADV can be estimated with two different ADVs, so six combinations of sensors are possible to use (1(2), 1(3), 2(1), 2(3), 3(1) and 3(2)). Two different estimations at each ADV height are plotted against each other (Figure 15) to distinguish whether the turbulence estimation depends on the ADV distance or not, since the distance between ADV1 and ADV3 is larger than between ADV1 and ADV2 .

In Figure 15 it can be seen that the values of $\bar{k}$ at the height of ADV1 are more or less equal if they are estimated with ADV 2 and ADV3. This implies that it does not matter whether the values of $\bar{k}_{1(2)}$ (or $k_{1(2)}$) or $\bar{k}_{1(3)}$ (or $k_{1(3)}$) are used for turbulence at the height of ADV1 in the turbulence problems. In the case of $\bar{k}_{3(1)}$ and $\bar{k}_{3(2)}$ the values of $\bar{k}$ are not equal. Here, the turbulence values estimated with ADV1 are larger than the values estimated with ADV2. It might seem that the distance between the ADVs is significant to estimate $\bar{k}$ in this case, because a larger ADV distance (3(1)) gives larger turbulence values than a small ADV distance (3(2)). However when $\bar{k}_{2(1)}$ and $\bar{k}_{2(3)}$ are compared, which have the same ADV distance, the use of ADV1 for the estimation of turbulence at ADV2 results in larger turbulence values compared to the estimations with the use of ADV3. From this it can be concluded that apparently the use of ADV1 in the estimation of turbulence velocities results in too large values. This might be caused by the vertical orbital motion effect of the waves. At the height of ADV1, the orbital motion is smaller compared to the orbital motion at the heights corresponding to ADV2 and ADV3. Therefore, also the orbital velocities are smaller at the height of ADV1 and the turbulent velocities become overestimated (equation 2). Anyway, it is better to use ADV2 and ADV3 to estimate turbulence velocities. Therefore, the following combinations are used; at the height of ADV1 turbulence is estimated with ADV2 (1(2)), at the height of ADV2 turbulence is estimated with ADV3 (2(3)) and at the height of ADV3 the turbulence is estimated with ADV2 (3(2)).

In most of the figures of this thesis, the turbulent kinetic energy is non-dimensionalized by the operation:

$$\bar{k}\,(-) = \sqrt{\bar{k}/gh} \qquad [5]$$

where g is the gravitational acceleration ($9.81\ m/s^2$) and h is the waterdepth at the position of the CRD instrument rig.

This parameter is used to recover the influence of different wave conditions and water levels on the data. So results of different hydrodynamic conditions can be compared.

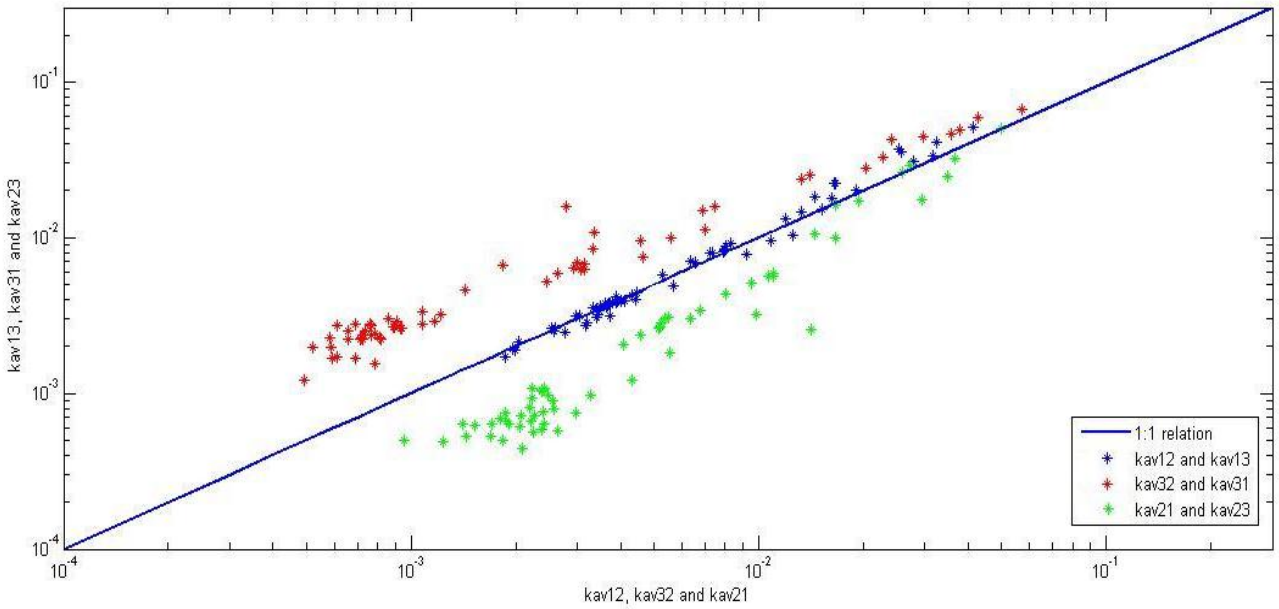

Figure 15: Comparison of the estimated time-averaged turbulent kinetic energy per unit mass (m^2s^{-2}). The blue solid line indicates equal values of $\bar{k}$, $\bar{k}_{1(2)}$ and $\bar{k}_{1(3)}$ (blue stars) show almost equal values, $\bar{k}_{3(2)}$ and $\bar{k}_{3(1)}$ (red stars) show larger values for $\bar{k}_{3(1)}$ and $\bar{k}_{2(1)}$ and $\bar{k}_{2(3)}$ (green stars) show larger values for $\bar{k}_{2(1)}$.

5.3.2 Cross-shore position of the turbulence-measuring frame

The cross-shore position of the turbulence-measuring frame is determined using a non-dimensional parameter, ζ. Here, an example of the cross-shore position of the turbulence measuring frame is given:

$$\zeta = \frac{x_{CRD} - x_0}{x_{BR} - x_0} \quad [6]$$

where x_{CRD} is the cross-shore position of the turbulence measuring frame, x_{BR} is the cross-shore position of the edge of the surfzone and x_0 is the shore-line.

The cross-shore positions are determined relative to the wave paddle. The cross-shore position of the CRD rig was constant during the entire experiment ($x_{CRD} = 64.952\ m$). However, the position of the surfzone and shoreline varied during the experiment with changing water level and wave conditions between individual runs. So these positions were determined for every single wave run. The value for x_{BR} is determined as the position between an increase in the short-wave significant wave-height H_s and the sudden decrease in H_s. This observation was combined with the position of where the short-wave energy dissipation D_w suddenly increases as well (Figure 16). For this purpose, H_s was determined using linear wave theory and D_w was defined using the model for steep beaches of Baldock et al. (2004):

$$D_w = \left[\alpha \frac{2\pi}{T} \rho g {H_{rms}}^2 / 8\pi\right] \cdot \left[\left(1 + \left(\frac{H_{max}}{H_{rms}}\right)^2\right) Q_b\right] \quad [7]$$

where breaker parameter $\alpha = 1$, T is the peak wave period, the water density $\rho = 1000\ kg/m^3$, the acceleration of gravity $g = 9.81\ m/s^2$, H_{rms} is the root-mean-square wave height, H_{max} is the maximum wave height and Q_b is the fraction of breaking waves.

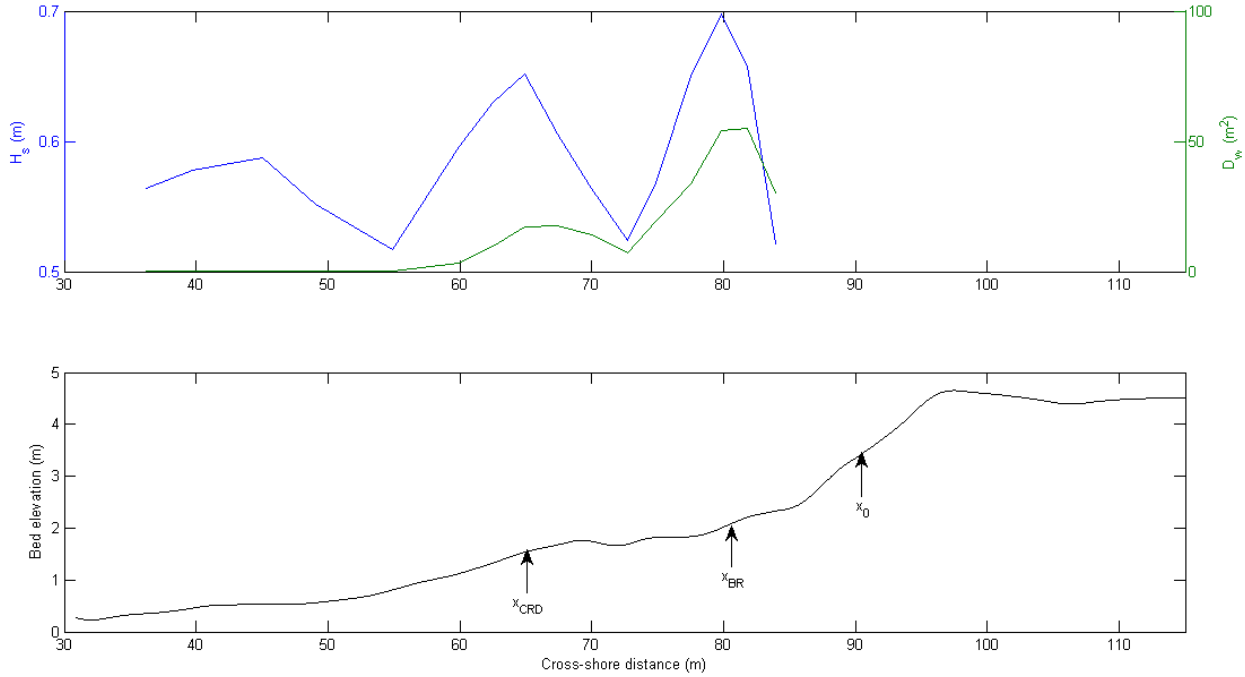

Figure 16: Definition of x_{CRD}, x_{BR} and x_0.

The reference point x_0 is determined as the position where the water depth is approximately zero, the shoreline (Figure 16). First, the run-averaged water depth at $x = 83.91\,m$ was defined using the pressure data of the PT transformed to the sea surface elevation and was added to the bed level at this location. This resulted in the water level relative to the bottom of the flume. This height above the bottom of the flume was extrapolated to the smoothed cross-shore profiles measured before the start of every run. The x-value of this height was determined as x_0. When $\zeta \approx 1$ the turbulence measuring frame was located at the edge of the surfzone, when $\zeta < 1$ it was located in the surfzone and when $\zeta > 1$ it was at a position seaward of the surfzone. Note that these allocations have no sharp boundaries, because random waves are used.

The parameter ζ was verified using visual observations of bores and breaking waves at different positions during various conditions (Figure 17). Near the edge of the surfzone ($\zeta \approx 1$), the number of breaking waves is larger than outside the surfzone or inside the surfzone. Additionally, inside the surfzone bores are more abundant compared to plunging breakers, whereas near the edge of the surfzone the plunging breakers are more prevailing.

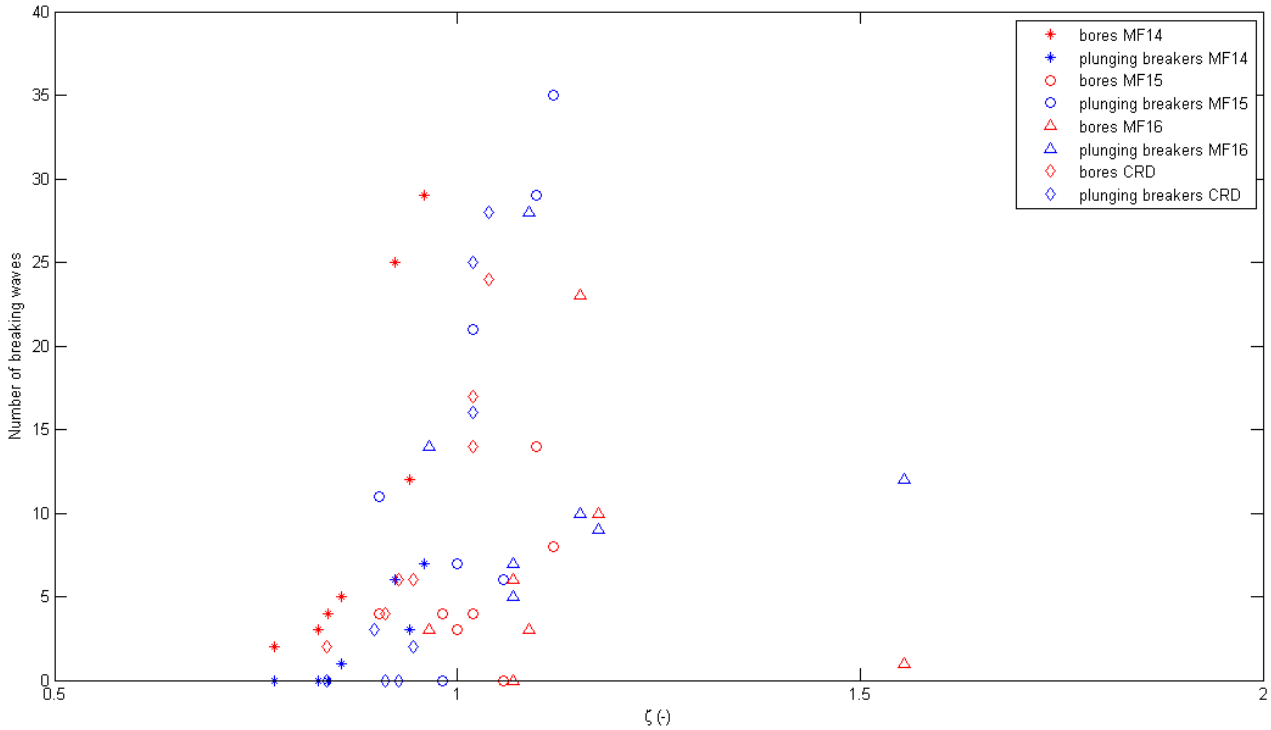

Figure 17: Counted number of bores and plunging breakers in relation to the cross-shore position.

5.3.3 Vertical profiles suspended-sediment concentrations

The vertical profiles of suspended sediment concentrations will be displayed with run-averaged values of the measured suspended-sediment concentrations at each height above the bed.

5.3.4 Relation between the turbulent kinetic energy and suspended sediment concentrations

A relation between the turbulent kinetic energy and suspended sediment concentrations can be determined using the instantaneous values of the nearbed turbulent kinetic energy (TKE) and suspended-sediment concentration (SSC). When a peak in the instantaneous TKE is shortly followed ($< 1\,T_p$) by a peak in SSC, it is assumed that turbulence stirs up the bed sediment. The determination of peaks in the instantaneous TKE and SSC can be defined using threshold values. It is difficult to determine a threshold value for the wave breaking-induced turbulence reaching the sea bed. Therefore it is chosen to follow a similar method used in Jaffe and Sallenger (1992) and Scott et al. (2009). Peak values both in the turbulent kinetic energy and suspended-sediment concentrations are defined with a threshold value determined by:

$$threshold = \mu + 3\sigma \qquad [8]$$

where μ is the run-averaged mean value and σ is the standard deviation of the wave run. For both the TKE and SSC data of the ADV and STM closest to the bed were used.

A binary scale was added for peak (above the threshold value) and non-peak values (below the threshold value). Peak values were set at a value of 1 and non-peak values were assigned as 0. The problem with this way of peak determination is that sometimes during one single turbulence or sediment suspension event the value of the turbulent kinetic energy or suspended sediment concentration drops below the threshold value and thus one single event of a long duration is determined as two separate shorter events. A solution for this problem is determined by a certain threshold time interval between two separate peak events. An example can be seen in Figure 18 (black circles) at time = $1.235*10^4$ s. The threshold time intervals are dependent on the peak wave period (T_p) of a wave run and are given in Table 2. If a time interval of non-peak values is smaller than or equal to the time interval threshold value, the non-peak values are set to a value of 1, which determines the presence of a peak value. In this way two separate defined peak events are merged to one single event (Figure 18, red stars).

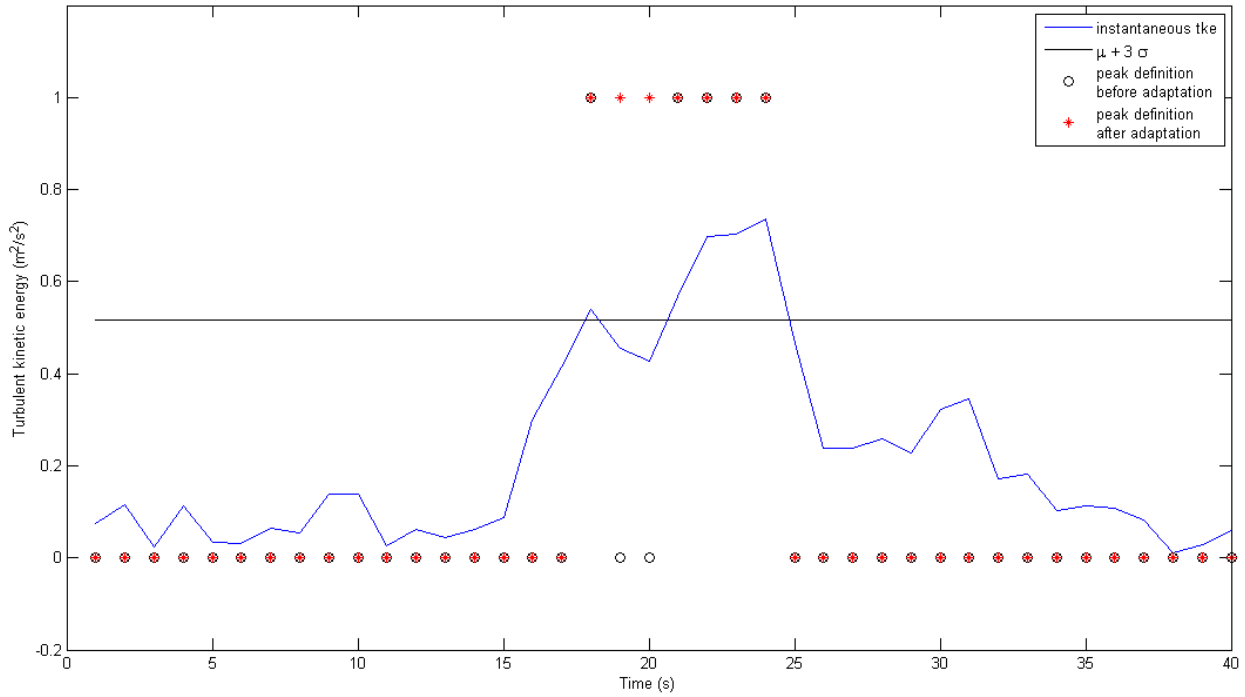

Figure 18: An example of the adaptation of the peak definition.

Table 2: Threshold time intervals for turbulent and sediment suspension peaks.

Threshold time intervals for TKE

T_p (s)	**F_s (Hz)**	**Threshold time steps (-)**	**Threshold time interval (s)**
7.1	10	2	0.2
7.7-8.5	10	3	0.3
8.7-12.9	10	4	0.4

Threshold time intervals for SSC

T_p (s)	**F_s (Hz)**	**Threshold time steps (-)**	**Threshold time interval (s)**
7.1-8.2	4	4	1
8.4-8.8	4	5	1.25
12.2-12.9	4	6	1.5

After the events of TKE and SSC were determined, it was tried to related these events. It was stated that an TKE and SSC event are related if the start of an SSC event occurs in less than one peak period after the centre of a TKE event:

$$SSC_{begin} - TKE_{centre} < 1\ T_p \quad [9]$$

This threshold is chosen because there is a lag between the occurrence of a TKE event and the following SSC event.

6. Turbulence under breaking waves

6.1 Cross-shore position and turbulent kinetic energy

It seems that there is a clear relation between run-averaged TKE values and cross-shore position (Figure 19). Seaward of the surfzone ($\zeta > 1$), the TKE is relatively small. Normalized TKE values for $\bar{k}_{1(2)}$ vary between 0.015 and 0.025. The values for $\sqrt{\bar{k}_{2(3)}/gh}$ and $\sqrt{\bar{k}_{3(2)}/gh}$ are slightly smaller and between 0.005 and 0.020. Landward of the edge of the surfzone ($\zeta < 1$), TKE values are low as well, and are comparable with the values of the position seaward of the surfzone. However, some values for $\bar{k}_{1(2)}$ are slightly larger at the landward side of the edge of the surfzone compared to the location seaward of the surfzone. This small difference might be due to the presence of spilling bores generated by waves which broke at the edge of the surfzone. The TKE at the edge of the surfzone ($\zeta \approx 1$) is several times higher (about 3 to 4 times), than at the other cross-shore positions. So at the edge of the surfzone, where wave breaking dissipation is the largest, the intensity of TKE is also the largest.

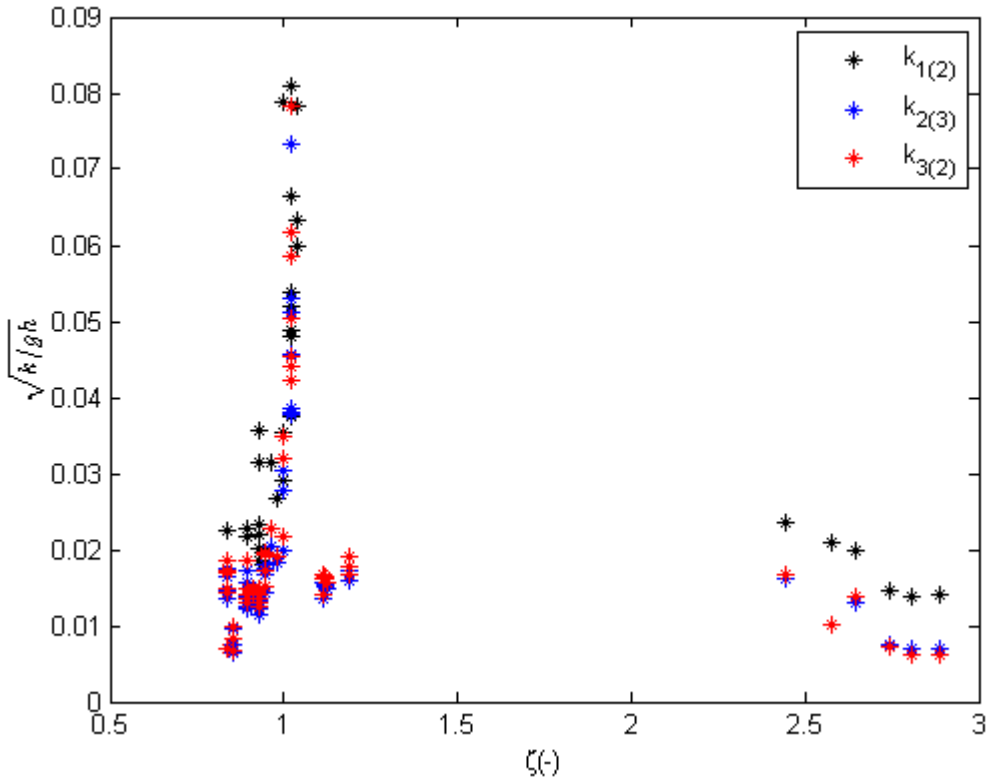

Figure 19: Non-dimensional turbulent kinetic energy against the relative cross-shore position.

6.2 Vertical structure of turbulence in the water column

The comparison between $\bar{k}_{1(2)}$ and $\bar{k}_{2(3)}$ (Figure 20) shows that the near-bottom turbulent kinetic energy is larger than the turbulent kinetic energy at the centered ADV for relatively small TKE intensities. When the TKE intensities of $\bar{k}_{1(2)}$ increase, the TKE values of $\bar{k}_{2(3)}$ increase as well. In some wave runs $\bar{k}_{1(2)}$ is equal to $\bar{k}_{2(3)}$ and in two wave runs $\bar{k}_{2(3)}$ is even larger than $\bar{k}_{1(2)}$.

The comparison between $\bar{k}_{1(2)}$ and $\bar{k}_{3(2)}$ (Figure 21) also shows that the near-bottom TKE is larger than the TKE at the top ADV for relatively small TKE intensities. However, the comparison of relatively large TKE intensities shows larger values for $\bar{k}_{3(2)}$ than for $\bar{k}_{2(3)}$ (Figure 22), whereas in the area with small TKE values the turbulent kinetic energy of $\bar{k}_{2(3)}$ and $\bar{k}_{3(2)}$ are equal. So, during conditions with relatively small TKE intensities, $\bar{k}_{1(2)} \gg \bar{k}_{2(3)}$ and $\bar{k}_{1(2)} \gg \bar{k}_{3(2)}$, where $\bar{k}_{2(3)} \approx \bar{k}_{3(2)}$. During conditions with larger TKE intensities, there is no clear relation between $\bar{k}_{1(2)}$ and $\bar{k}_{2(3)}$, because $\bar{k}_{1(2)}$ can be larger, equal or smaller compared to $\bar{k}_{2(3)}$. The upper part of the vertical turbulence structure during intense turbulence conditions shows a more clear relation: $\bar{k}_{1(2)} < \bar{k}_{3(2)}$ and $\bar{k}_{2(3)} < \bar{k}_{3(2)}$.

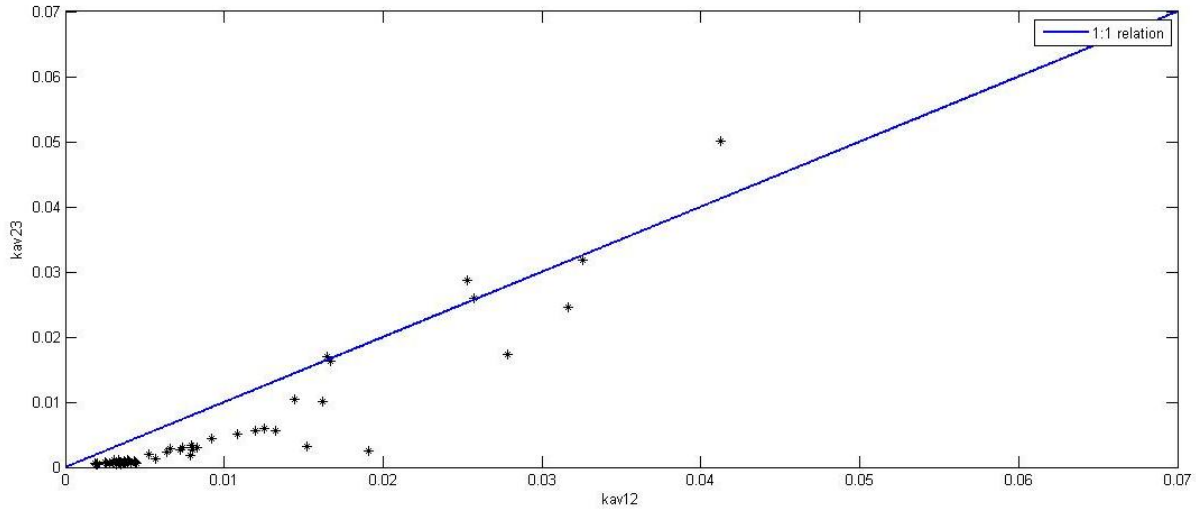

Figure 20: The comparison of $\bar{k}_{1(2)}$ and $\bar{k}_{2(3)}$ (black stars). Values where $\bar{k}_{1(2)}$ and $\bar{k}_{2(3)}$ are equal are indicated with the blue solid line.

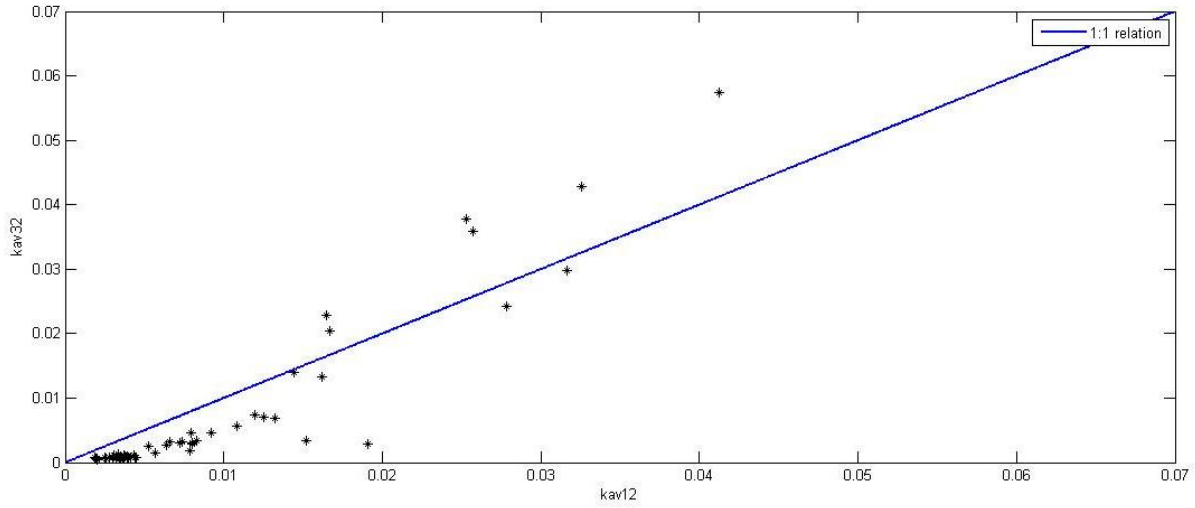

Figure 21: The comparison of $\bar{k}_{1(2)}$ and $\bar{k}_{3(2)}$ (black stars). Values where $\bar{k}_{1(2)}$ and $\bar{k}_{3(2)}$ are equal are indicated with the blue solid line.

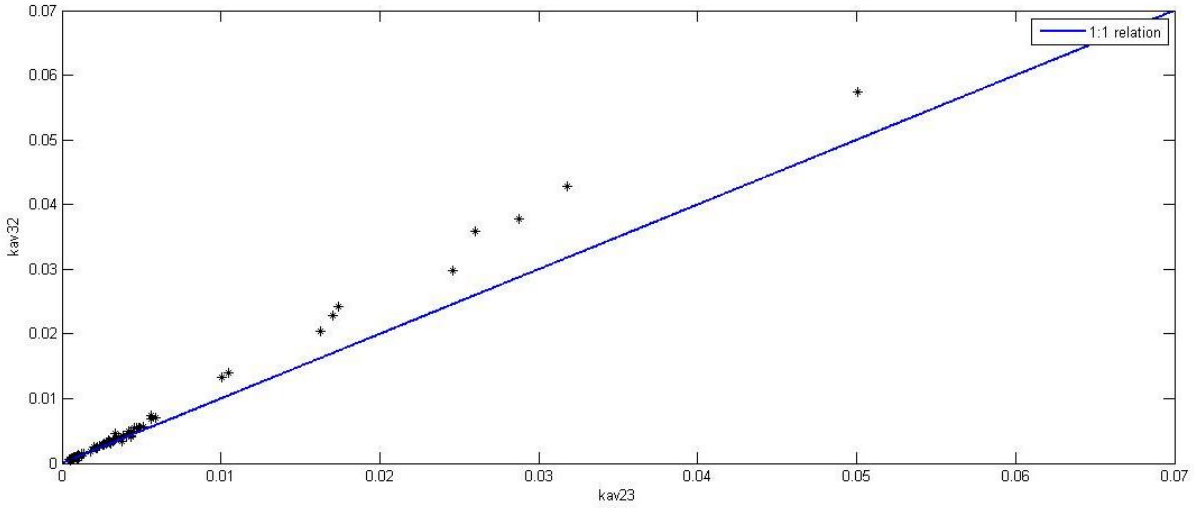

Figure 22: The comparison of $\bar{k}_{2(3)}$ and $\bar{k}_{3(2)}$ (black stars). Values where $\bar{k}_{2(3)}$ and $\bar{k}_{3(2)}$ are equal are indicated with the blue solid line.

The observed relation between $\bar{k}_{1(2)}$, $\bar{k}_{2(3)}$ and $\bar{k}_{3(2)}$ is clearly visible in the vertical TKE profiles (Figure 23). The general trend of increasing TKE relative to increasing relative water depth of the ADVs is very obvious. An increased relative water depth indicates small water depths, which are related to large wave breaking intensities. Whereas a small relative water depth is related to less intensive or non wave breaking conditions.

Also, the structure of the vertical TKE profiles show differences with the varying TKE intensities. To make an indication of the structure related to the position in cross-shore direction, the vertical profiles are classified in three groups. These groups are: the edge of the surfzone (black lines), landward of the edge of the surfzone (red lines) and seaward of

the surfzone (blue lines). Almost all TKE profiles at the edge of the surfzone have high TKE intensities and are of the structure $\bar{k}_{1(2)} < \bar{k}_{3(2)} > \bar{k}_{2(3)}$. However, sometimes the structure $\bar{k}_{1(2)} \geq \bar{k}_{3(2)}$ and $\bar{k}_{1(2)} > \bar{k}_{2(3)} < \bar{k}_{3(2)}$ occurs during these conditions. The increase of the turbulent kinetic energy near the bottom might be caused by the presence of large ripples, which will be elaborated in the discussion.

The increase of the TKE on top of the vertical profile ($\bar{k}_{3(2)}$) refers to a turbulence source at the top of the water column, whereas an increase of TKE values near the bottom ($\bar{k}_{1(2)}$) refers to a turbulence source near the bottom. So the vertical turbulence structure of the conditions at the edge of the surfzone define conditions with the dominance of surface generated turbulence which is due to the breaking of waves. The classes further from the edge of the surfzone show different vertical turbulence profiles. During these conditions (red and blue) the vertical structure of the run-averaged turbulent kinetic energy is $\bar{k}_{1(2)} \gg \bar{k}_{2(3)}$, $\bar{k}_{1(2)} \gg \bar{k}_{3(2)}$ and $\bar{k}_{2(3)} \approx \bar{k}_{3(2)}$. This signifies the greater importance of near-bed generated turbulence relative to the surface generated turbulence. There is only a slight difference between the vertical profiles of the locations landward and seaward of the edge of the surfzone (red and blue, respectively). The TKE intensities are slightly larger for conditions landward of the edge of the surfzone compared to conditions seaward of the surfzone. This difference might be caused by the fact that small waves are breaking and bores are present (Figure 17) inside the surfzone. These bores and small breaking waves may generate more turbulence compared to outside the surfzone where wave breaking hardly occurs.

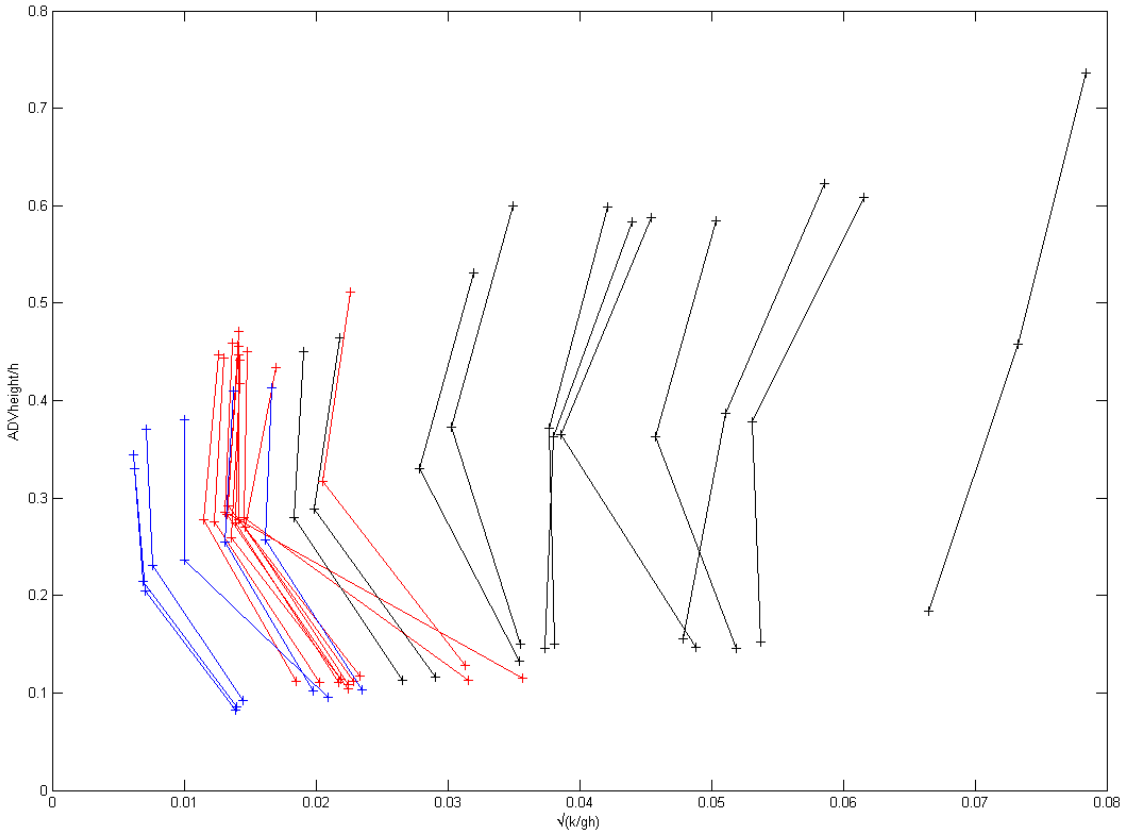

Figure 23: Vertical profiles of the time-averaged turbulent kinetic energy inside the surfzone (black lines), landward of the surfzone (red lines) and seaward of the surfzone (blue lines).

7. Sediment suspension due to breaking-induced turbulence

7.1 General observations of sediment suspension

7.1.1 Suspended-sediment concentrations and cross-shore position

The suspended sediment concentrations are dependent on the relative cross-shore distance (Figure 24). Around and at the edge of the surfzone, the run-averaged SSCs can reach high values of about $6 - 7\ kg/m^3$ near the sea bed (z = 0.040 m and z = 0.035 m). The SSCs outside the surfzone ($\zeta > 1$) and inside the surfzone ($\zeta < 0.8$) are generally smaller. However, there is an increase in SSC between $\zeta = 2$ and $\zeta = 2.5$.

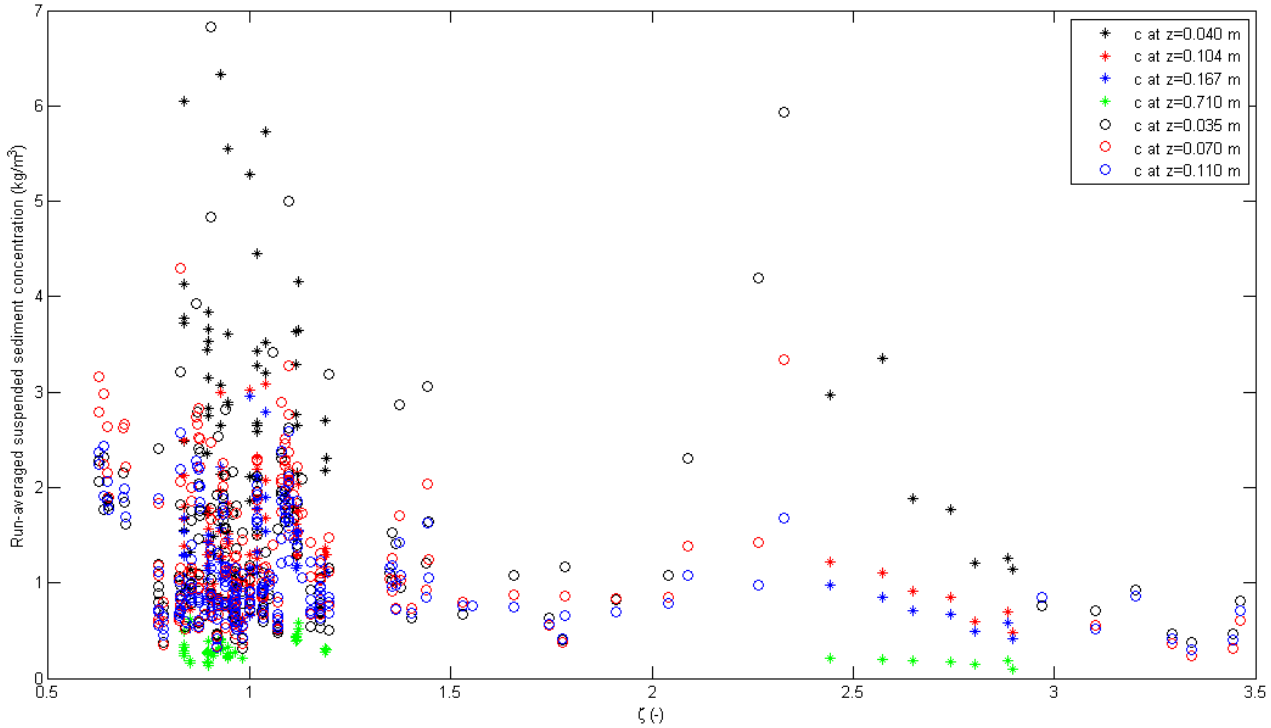

Figure 24: Run-averaged suspended sediment concentration (kg m^{-3}) at z=0.040 m (black stars), z=0.104 m (red stars), 0.167 m (blue stars) and 0.710 m (green stars) above the bed, and at z=0.035 m (black circles), z=0.070 m (red circles) and z=0.110 m (blue circles) against the relative cross-shore distance of the turbulence measurements (-).

Both at the edge and outside the surfzone, SSCs increase near the seabed. A further descent into the water column shows larger differences between the suspended sediment concentrations. The range of SSC near the bottom (z = 0.040 m and z=0.035 m) is much larger than the range at a higher elevation in the water column (z = 0.710 m). It also can be recognized that the pattern of SSCs far outside the surfzone ($\zeta > 2.5$) has a quite constant decrease relative to the increase of distance from the surfzone edge. However, around the edge of the surfzone this pattern is more chaotic. There are very high but also low SSC for a certain position. This might be caused due to the fact that wave conditions were more variable in wave height and water depth in here, whereas far from the surfzone edge there

was only one wave condition for each cross-shore position. The increase in SSC between $\zeta = 2$ and $\zeta = 2.5$ might be caused by the presence of ripples or it may be caused by numerous clouds of advected suspended sediment. This will be further elaborated in the discussion.

7.1.2 SSC profiles related to cross-shore position

The magnitude of SSCs and the structure of vertical SSC profiles differ depending on cross-shore position (Figure 25). Suspended sediment concentrations at the edge of the surfzone (CRD) can reach values of 5 – 5.5 kg/m^3 and outside the surfzone (MF14, MF15 and MF16) sediment concentrations range between 1 and 3 kg/m^3. The vertical concentration profiles of CRD and MF14 show a similar near bed structure, suspended sediment concentrations are strongly increasing towards the bed. The difference between the near-bed profiles of CRD and MF14 is solely the magnitude of the suspended sediment concentrations. The concentrations at CRD are about 2 times higher compared to MF14. The upper part of the vertical suspended sediment profile of CRD cannot be compared to the other profiles, but it can be recognized that the upper part of the CRD profiles is different from the near-bed part. Near the bed (z ≈ 0 – 0.10 m), CRD shows a strong gradient in the suspended sediment concentration. However, this gradient is almost zero in the upper part of the vertical profile (z ≈ 0.10 – 0.17 m). Additionally, SSCs are still significantly high in the upper part of the CRD profile.

MF15 and MF16 do not only show small values of suspended sediment concentrations, but they also have a different vertical structure compared to CRD and MF14. The gradient between z = 0.035 and 0.105 m is almost 0 and thus the SSC is quite constant over water depth.

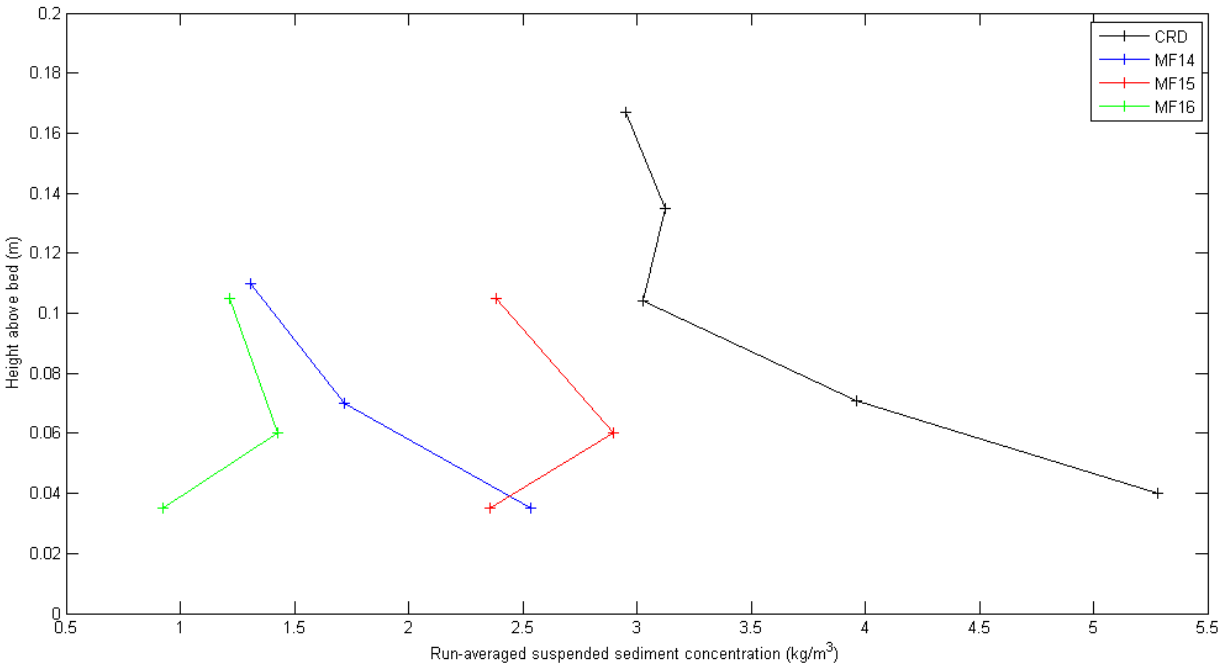

Figure 25: Vertical profiles of the run-averaged suspended sediment concentrations at different positions in cross-shore direction during experiment C2 condition 09. In this case CRD (black) is situated at the edge of the surfzone, MF14 (blue) is situated seaward of CRD and MF15 (red) and MF16 (green) are at the landward side of the CRD.

7.2 Relation between TKE events and SSC events

7.2.1 Occurrence of TKE peak events and SSC peak events

The occurrence of intense turbulent events near the sea bed is intermittent (Figure 26, lower panel). Not every passing wave results in an intense turbulent event near the sea bed. It can be seen that large disturbances in the cross-shore and vertical turbulent velocities are related to large intense turbulent events. For example, a large disturbance can be recognized just before time = $2.1921*10^6$ sec (Figure 27 (detailed)). The intense turbulent events seem to occur during the passage of a wave trough and has stopped during the passage of the next wave crest. The occurrence of intense sediment suspension events is intermittent as well (Figure 28). However, not every peak in SSC can be related to a large event in TKE. Sometimes SSC peaks occur when there is no peak in TKE (near the end of the run). Occurring peaks in SSC without the presence of a TKE peak can be explained by advection of waves breaking further onshore.

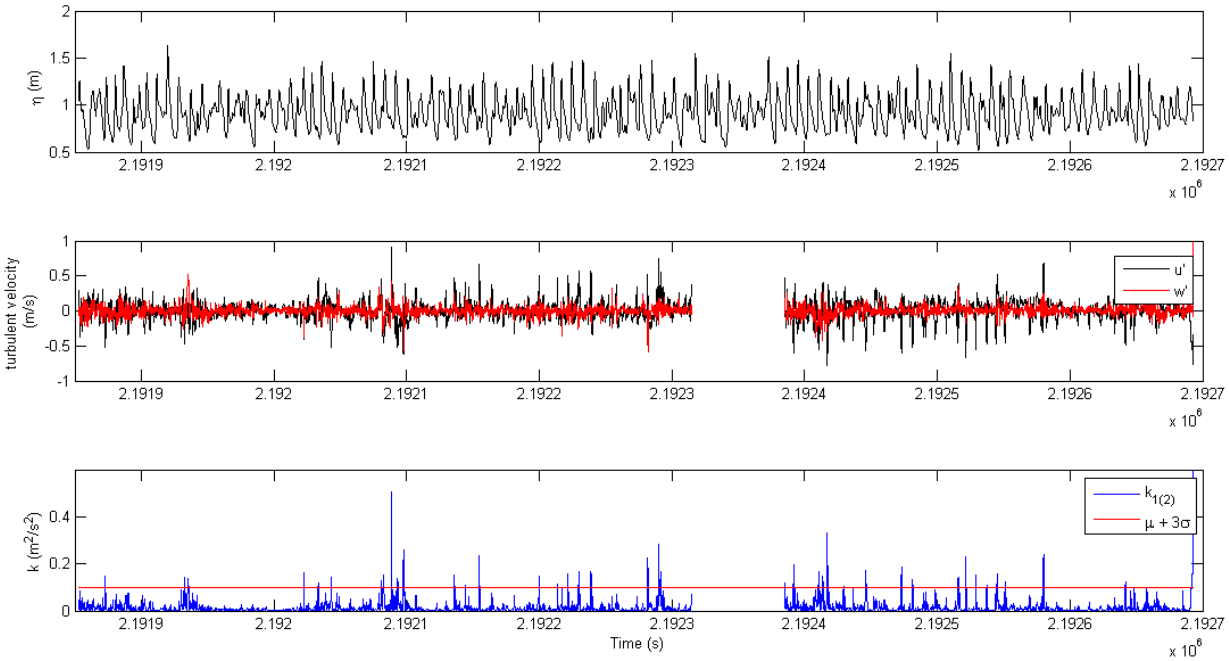

Figure 26: Water surface elevation at the turbulent measuring frame (upper panel), the cross-shore and vertical turbulent velocities u' (black line, middle panel) and w' (red line, middle panel) and the turbulent kinetic energy (blue line, bottom panel). The threshold value for intense turbulent events near the sea bed is indicated with the red line in the bottom panel. This figure is an example of wave run B2 condition c01, $\zeta = 1$.

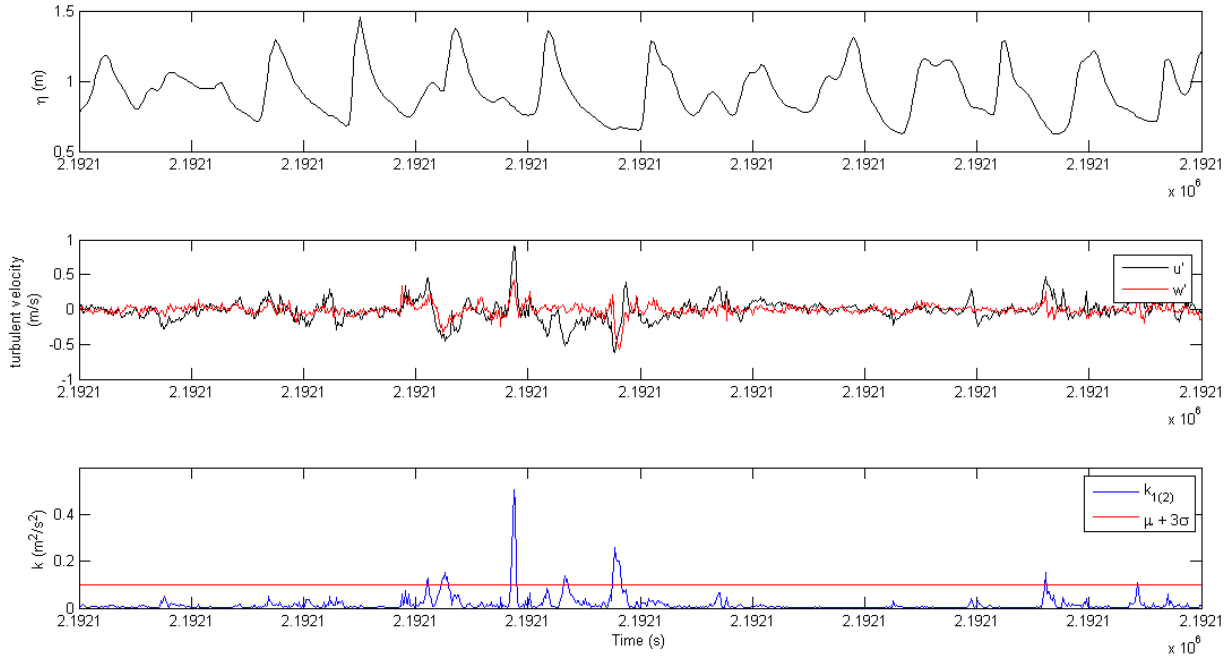

Figure 27: Same as Figure 26, but this is a detailed image of the intense turbulent event around time = 2.1921*10^6 sec.

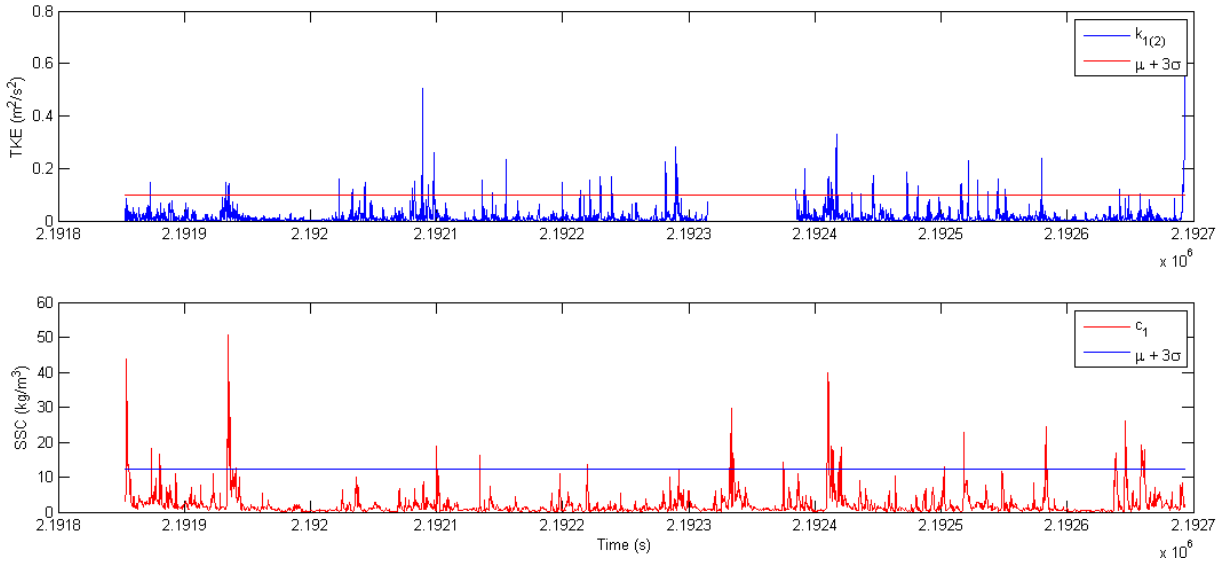

Figure 28: Turbulent kinetic energy events (upper panel) and suspended sediment events (lower panel). This figure is an example of wave run B2 condition c01, $\zeta = 1$.

7.2.2 Relation between TKE and SSC

On average, an increasing time-averaged near-bed TKE is related to an increased mean near-bed SSC (Figure 29). A distinction in the increasing pattern can be recognized around $\sqrt{\bar{k}_{1(2)}/gh} \approx 0.025$. With low intensity turbulent conditions ($\sqrt{\bar{k}_{1(2)}/gh} < 0.025$), the increase in the suspended sediment concentrations is rapid. In cases where $\sqrt{\bar{k}_{1(2)}/gh} > 0.025$, the increase of suspended sediment is more gradual with increasing turbulent kinetic energy. The concentrations start at the same level as for the mean sediment concentrations during very low turbulent intensities and then increase gradually to large concentrations.

For the indication of cross-shore position, the data is subdivided in three different classes. There are some remarkable points to make. One observation is that there are no surfzone data for $\sqrt{\bar{k}_{1(2)}/gh} < 0.025$, but there are some data landward and seaward of the surfzone for $\sqrt{\bar{k}_{1(2)}/gh} > 0.025$. There is a remarkable red data point near the concentration of $c = 6.5\ kg\ m^{-3}$. This point does not follow any of the two patterns. The instantaneous TKE and SSCs of this wave run are shown in Figure 30. It can be seen that SSCs are already very large in the beginning of the wave run, whereas the TKE is not significantly present at this stage of the run. Therefore the vast sediment concentrations at the beginning of this wave run needs to be caused by another reason than an enhanced turbulent kinetic energy due to breaking waves. Advection of sediment may play a role in this. How the presence of sediment advection can be investigated will be explained in the discussion. It can also be

recognized that the data for near-bed sediment concentration do not drop to zero (Figure 30). This might point at an error in the processing of the data, or the sensor is partly disappearing in the bed (z < 0.04 m).

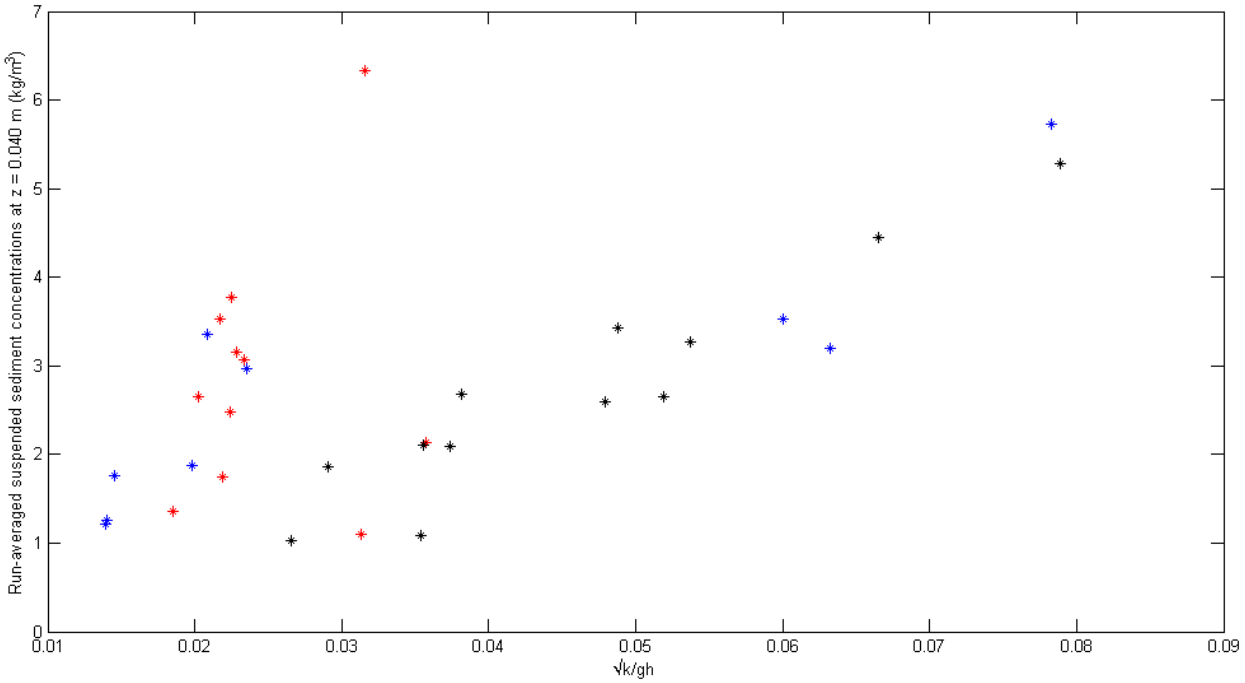

Figure 29: Run-averaged suspended sediment concentration against the near-bed run-averaged turbulent kinetic energy at ADV1 inside the surfzone (blue), landward of the surfzone (blue) and seaward of the surfzone (red).

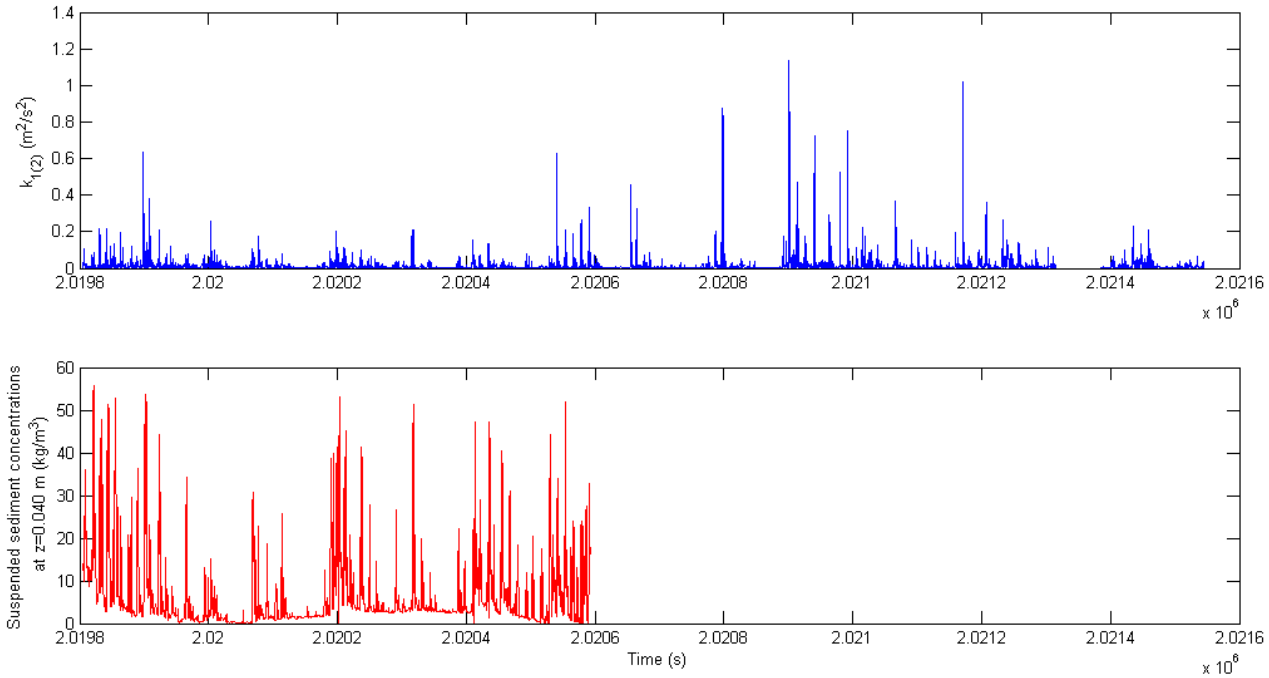

Figure 30: $k_{1(2)}$ (upper panel) and near-bed suspended sediment concentrations (bottom panel) during wave run A8, condition c01.

7.2.3 Relation between TKE events and SSC events

There is no clear relation between the number of peaks in the TKE and the number of peaks in SSC (Figure 31) with the emphasis on the fact that the peaks in SSC would increase if the amount of peaks in the TKE are higher. This is not the case. However, it can be recognized that the number of peaks in SSC only exceeds the number of peaks in the TKE when the number of TKE peaks is small. Despite of the constant number of SSC events, which varies between 20 and 60 events per wave run, the number of TKE events shows a larger range and is increasing up to 160 events per wave run. The difference between the TKE and SSC events is the way the events are generated. The TKE events are generated by turbulence originating from the SBL (or BBL). This process is locally induced by either breaking waves or the orbital wave motion. The SSC events can be generated locally due to wave breaking turbulence hitting the sea bed and vortex shedding caused by ripples, but the high concentrations can also represent passing sediment clouds transported due to advection. Because non-local mechanisms play an additional role next to turbulence in the generation of SSC peaks, the number of SSC peaks and TKE peaks has no 1:1 relation.

There is no clear relation between the short-wave energy dissipation and the percentage of TKE events which can be related to SSC events (Figure 32). There is no clear structure of the data points. On average, the percentage of related events is quite constant in relation to the short-wave energy dissipation. The average of the related event percentages is 44.31%, which means that on average 44.31% of the TKE events is followed by an SSC event in less than 1 T_p. Scott et al. (2009) found a relation of 37% for an accretive case and 22% for an erosive case, which are smaller values than the values found here. It was also observed that both the turbulent kinetic energy (Figure 19) and suspended-sediment concentrations (Figure 24) are related to the cross-shore position and thus the degree of wave breaking. Therefore it is expected that an increase in the short-wave energy dissipation would be related to a larger percentage of related events, since the dissipation is generated by breaking waves. It might be that the data points of conditions away from the edge of the surfzone are too much influenced by the BBL. This might result in a lot of SSC events which are induced by bottom generated turbulence and become accidently related to a turbulence event. Therefore, only the conditions near the edge of the surfzone are highlighted in red (Figure 32). These data do not show a clear relation as well. However, the data near the surfzone edge shows an averaged percentage of related events of 37.95%, which is a comparable value with the results of Scott et al. (2009).

In the discussion it is further elaborated how the chosen threshold values and window size affects the results.

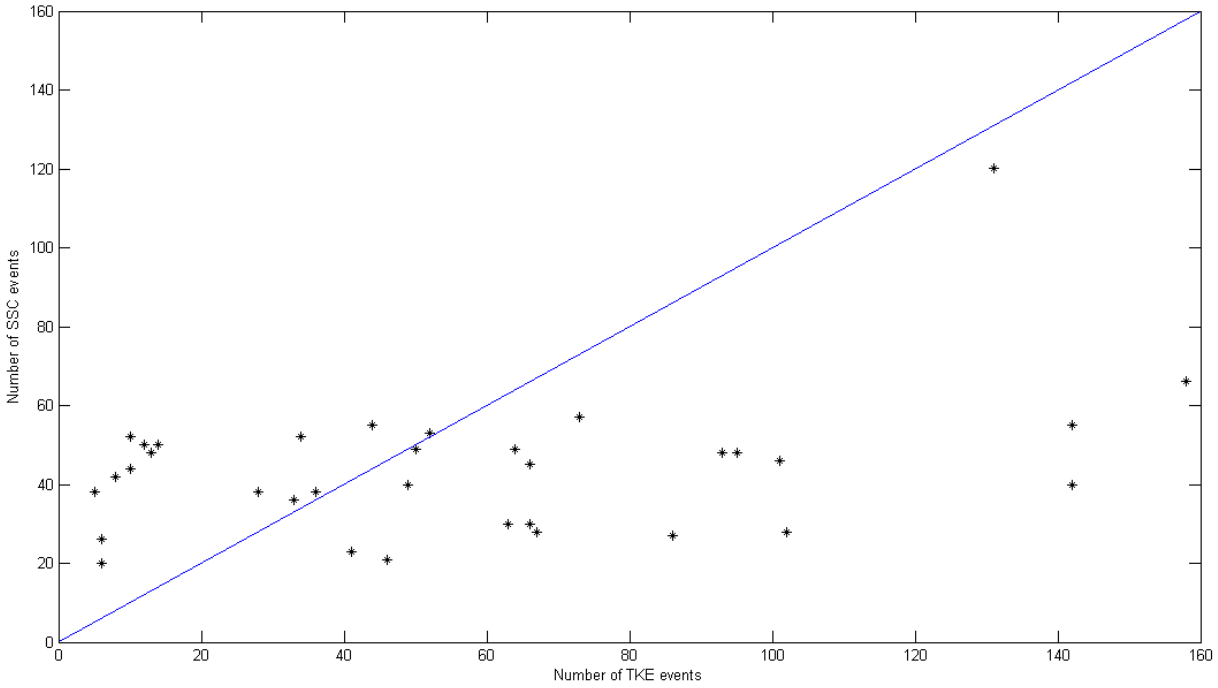

Figure 31: Relation between the number of peaks in TKE and the number of peaks in SSC determined by the threshold values of a certain wave run. The black line represents the 1:1 relation.

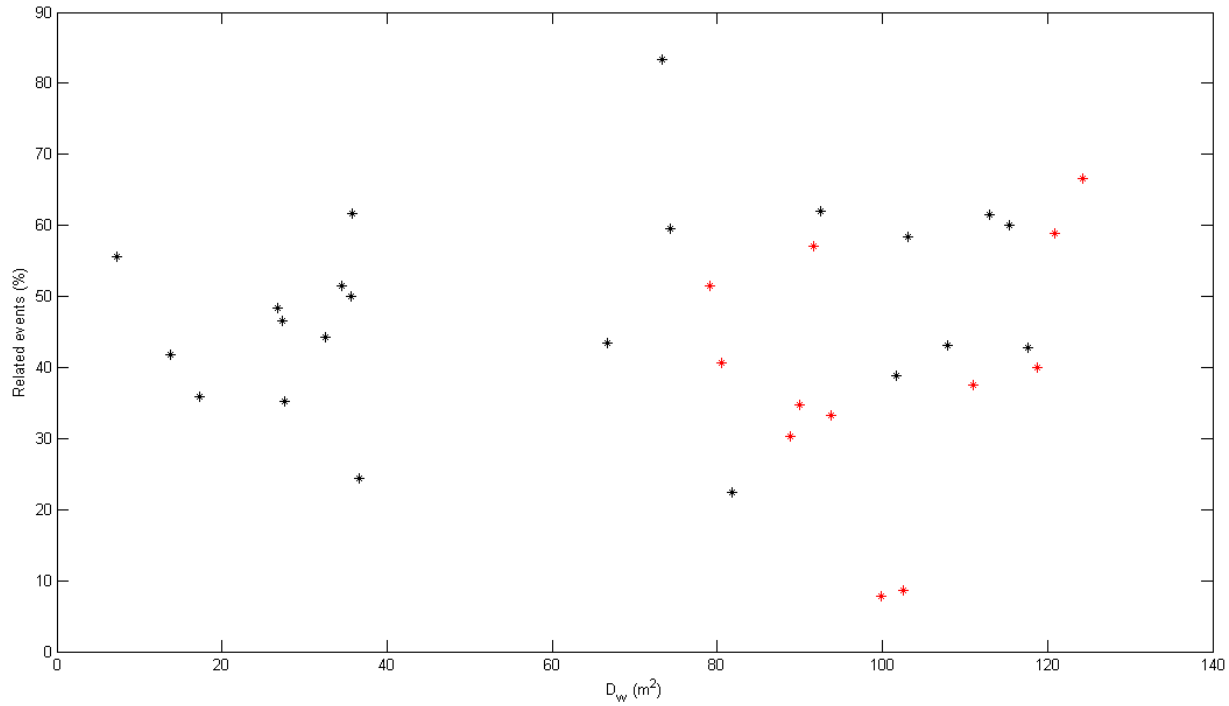

Figure 32: Relation between the percentage of TKE events which can be related to a SSC event and the short-wave dissipation. Conditions near the edge of the surfzone are coloured red ($\zeta \approx 1$). Threshold value $\mu + 3\sigma$ and window size $1T_p$.

8. Discussion

8.1 Turbulence under breaking waves; cross-shore and vertical variation of $\bar{k}$

The run-averaged turbulent kinetic energy is clearly related to the cross-shore position in the surfzone, as shown in Figure 19. At the edge of the surfzone the turbulent kinetic energy is 3 to 4 times higher than outside the surfzone. Scott et al. (2005) found that the time-averaged turbulent kinetic energy was the largest at the locations where most waves were breaking. This is in comparison with the results found here. Here, the edge of the surfzone is generally the position where the largest waves were breaking and plunging breakers were prevailing over bores, resulting in intense turbulent conditions. Therefore, the results are also similar to the results of Ruessink (2010), who found that fully wave-breaking conditions were related to larger Reynolds stresses than during weakly and non wave-breaking conditions. Also the results of Grasso and Ruessink (2011) show larger dissipation rates during fully breaking conditions.

The vertical structure of $\sqrt{\bar{k}/gh}$ during intense turbulent conditions differs from the vertical structure during less turbulent conditions, which in turn is related to the cross-shore position. Outside the surfzone and landward of the surfzone edge, the near-bed ($z/h \approx 0.1$) $\sqrt{\bar{k}/gh}$ is much larger than both the centred ($z/h = 0.2 - 0.3$) and top ($z/h = 0.4 - 0.5$) $\sqrt{\bar{k}/gh}$. The centred and top $\sqrt{\bar{k}/gh}$ are approximately equal. During intense turbulent conditions, located near the edge of the surfzone, usually both the near-bed ($z/h \approx 0.15$) and centred ($z/h > 0.3$) $\sqrt{\bar{k}/gh}$ are smaller than the top ($z/h > 0.5$) $\sqrt{\bar{k}/gh}$. However, sometimes the near-bed $\sqrt{\bar{k}/gh}$ is larger than or equal to the top $\sqrt{\bar{k}/gh}$ such that $\sqrt{\bar{k}/gh}$ increases from the centred $\sqrt{\bar{k}/gh}$ to both the bottom and top of the vertical TKE profile. This may be due to the presence of large ripples.

The ratio of the ripple height over ripple length (ripple steepness) was always larger than 0.01, except for 1 wave condition near $\zeta \approx 1$, thus ripples were present during each wave run (Figure 33). Figure 34 shows the large ripples around the measuring instruments when the water was removed after all wave runs. Such large ripples might induce vortex shedding, which may result in increased near-bed turbulence.

Since an increasing $\sqrt{\bar{k}/gh}$ at the top relative to the centred $\sqrt{\bar{k}/gh}$ indicates the dominance surface-generated turbulence, the vertical turbulence structures near the edge of the surfzone indicate that the breaking-induced turbulence is the most important source for turbulence in the water column. Further away from the edge of the surfzone, both landward and seaward, the vertical turbulence structures show an increase in $\sqrt{\bar{k}/gh}$ towards the bed. This signifies the relative importance of bed-generated turbulence induced by the bottom

boundary layer. Although they used the turbulence dissipation rate as a measure for turbulence, Grasso and Ruessink (2011) have also shown that the surface-generated turbulence plays an important role during fully wave-breaking conditions and that turbulence generated near the bed due to the bottom boundary layer increases with decreasing wave-breaking conditions.

Near the edge of the surfzone, the $\sqrt{\bar{k}/gh}$ values are larger than 0.025, whereas at the other locations $\sqrt{\bar{k}/gh}$ is smaller than 0.025. The observations of Yoon and Cox (2010) also showed $\sqrt{\bar{k}/gh}$ values larger than ~0.025 under breaking waves and were increasing upwards in the water column.

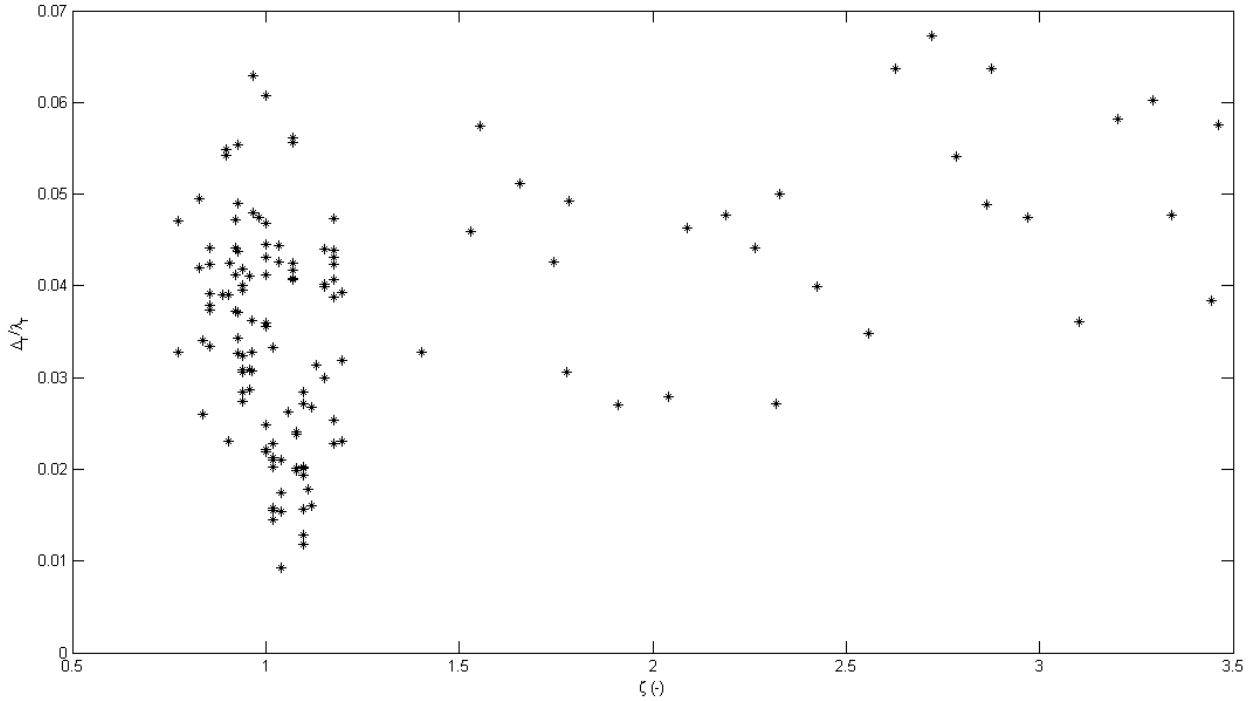

Figure 33: Ripple height to ripple length ratio for different cross-shore positions.

Figure 34: Large ripples around measuring instruments.

8.2 Sediment suspension in relation to cross-shore position

Mean suspended-sediment concentrations can reach very high values at the edge of the surfzone ($\zeta = 1$) compared to other cross-shore positions. However, outside the surfzone between $\zeta = 2$ and $\zeta = 2.5$ there is a deviation with high mean suspended-sediment concentrations as well. These latter high values may be caused by the presence of large ripples over here. The ripple steepness over here ranges between 0.025 and 0.050 (Figure 33). These large ripples might create sediment suspension in vortex shedding if the measuring instruments are located in the trough of a ripple. Another cause of the high mean concentrations might be the passage of numerous sediment clouds, which are advected by the undertow of breaking waves further landward. If advection took place and what the contribution of advected sediment is on the total suspended sediment concentration can be investigated using video data. In this way the presence, velocity and direction of sediment clouds can be observed. The measured SSC at another measuring point combined with the velocity of the sediment cloud can predict the timing of arrival of the sediment cloud in another location. If the timing and location of the SSC event is in agreement with the calculated timing and location, it can be concluded that the SSC event is an advected sediment cloud. Using the velocity of the undertow current is another way to determine advection. This can be used in a comparable way as the video data, but here the velocity of the sediment cloud is equal to the undertow of the broken wave, which can be calculated using Svendsen (1984).

Additionally, the suspended sediment concentrations can dramatically increase if the data processing went wrong or the sensor is located too close to the bed, as it was mentioned using Figure 30.

The structure of the sediment concentration profile in at the surfzone edge consist of mainly two parts. The gradient in suspended-sediment is very low in the upper part of the water column, but shows a strong increase near the bed. Suspended-sediment concentrations are still large in the upper part of the concentrations profile. From this it can be concluded that breaking waves cause larger sediment concentrations and the sediment is stirred up higher in the water column, compared to areas where less or no waves are breaking. Thus breaking-induced turbulence enhances the vertical mixing in the water column. These results were also observed by Ogston and Sternberg (2002). There are no observations of the upper water column of the other cross-shore locations. However, these concentrations would be smaller compared to the concentrations at the surfzone edge, because suspended-sediment concentrations tend to decrease in the upper water column and their mean near-bed concentrations are already small.

8.3 Relation between TKE events and SSC events

There is no clear relation between the short-wave energy dissipation and the percentage of TKE events that can be related to SSC events (Figure 32). Above, it was observed that both the turbulent kinetic energy and suspended-sediment concentrations are related to the cross-shore position and thus the degree of breaking waves. Therefore it is remarkable that a larger short-wave energy dissipation is not related to a larger percentage of related events since the dissipation is generated by breaking waves.

The absence of a relation might be caused due to the fact that all conditions are taken into account, including the conditions where bottom-generated turbulence was prevailing. During these latter conditions, the influence of large ripples might be too large and induce sediment suspension events. Therefore, these conditions need to be cancelled from this analysis. This was done using the ripple steepness around the measuring instrument frames during different conditions. The ripples were determined by subtracting the smoothed cross-shore profile from the non-smoothed cross-shore profile. From a section 5 meters before and after a certain measuring frame, the mean ripple height (Δ_r) and mean ripple length (λ_r) were determined and then divided, which resulted in the ripple steepness Δ_r/λ_r.

There is a small relation between the ripple steepness and cross-shore position (Figure 33). Around the relative cross-shore position of $\zeta \approx 1$, the ripple steepness is ranging between 0.01 and 0.07. Whereas further landward ($\zeta < 1$), the ripple steepness is between 0.02 and 0.05. Seaward of the surfzone only ripples with a large steepness are present, ranging between 0.025 and 0.07. During high turbulent intensities ($\sqrt{\bar{k}_{1(2)}/gh} > 0.04$), the ripple steepness seems to be limited by the value 0.025 (Figure 35). The high turbulent intensities

of $\sqrt{\bar{k}_{1(2)}/gh} > 0.04$ occur near the relative cross-shore position of $\zeta \approx 1$ (Figure 19), just like the small ripple steepness. Herewith, two threshold values were designed to filter the conditions with high turbulence intensities and relatively little influence by bedforms. For the ripple steepness the threshold value was chosen at 0.02 and the threshold value for $\sqrt{\bar{k}_{1(2)}/gh}$ was taken at 0.04. Unfortunately, this filter did still not result in a good relation between the short-wave dissipation and the percentage of TKE events which are related to SSC events (Figure 36).

Another cause might be that the threshold values to determine the TKE and SSC events are too small. For example in Figure 26, there are a lot of small peaks topping just above the threshold value. In this way all these relatively small events are included with the less frequent large events. So with a larger threshold value, only extremely large values are determined as events. The chosen window size might also affect the relation between TKE and SSC events. If the window size is too large, there is a larger chance that a SSC event, which is not induced by a TKE event hitting the sea bed, is accidently related to a TKE event. This might result in an overestimation of related events.

To investigate the influence of the chosen threshold value, the relation between TKE and SSC events is recalculated with the threshold $\mu + 4\sigma$ and a window size of $1T_p$ (Figure 37). This still did not result in a clear increasing pattern. However, when only taking the conditions near the surfzone edge into account, the pattern of related events is somewhat increasing with increasing dissipation. The average of the related events percentages for all conditions dropped to 42.55% and for the conditions near the surfzone edge this was 35.31%.

To investigate the influence of the chosen window size, the results are also shown in Figure 38 with a threshold value of $\mu + 4\sigma$ and a window size of $0.75\ T_p$. Comparable to Figure 32, the data of the related events seems quite constant and does not show a clear pattern. In this case the average percentage of related events is dropped to 38.28% for all data and 31.26% for conditions near the surfzone edge.

From this it can be concluded that the relation between the percentage of related TKE and SSC events and the short-wave energy dissipation is sensitive to the threshold value used to determine the events. A larger threshold value results in a better relation for conditions near the surfzone edge.

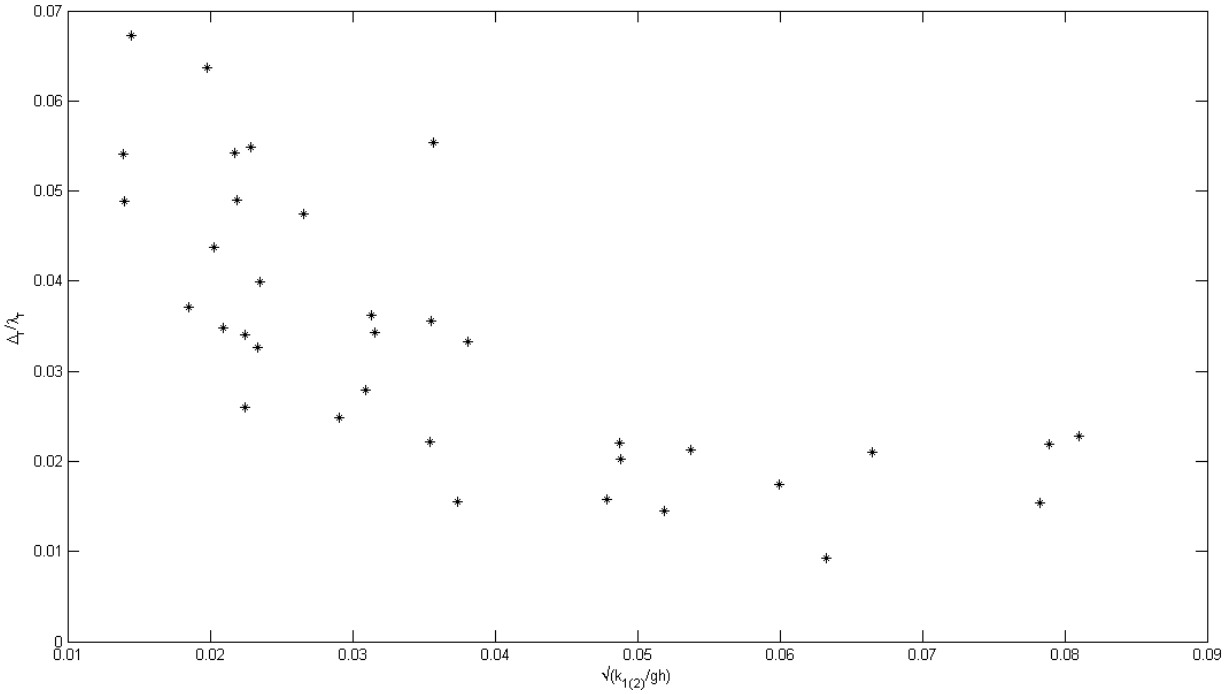

Figure 35: Ripple steepness against the near-bed$\sqrt{\bar{k}/gh}$.

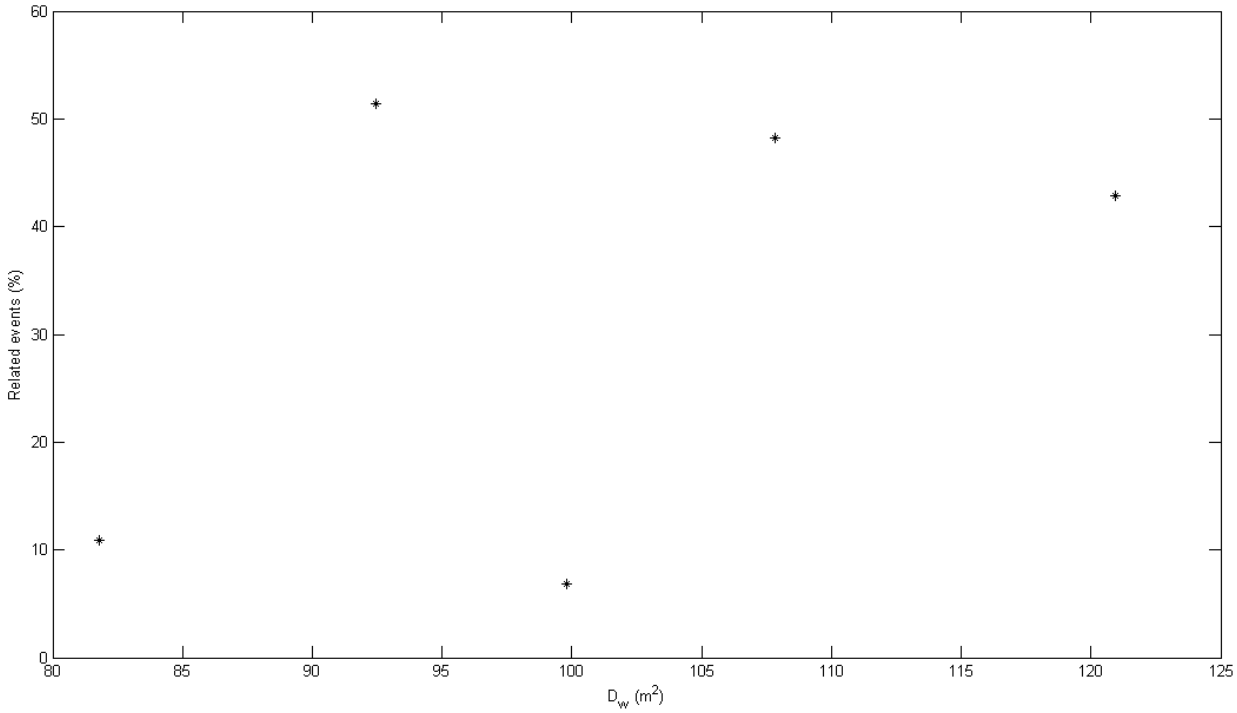

Figure 36: Relation between the percentage of TKE events which can be related to a SSC event and the short-wave dissipation for the filtered conditions with $\sqrt{\bar{k}_{1(2)}/gh} > 0.04$ and ripple steepness < 0.02 m.

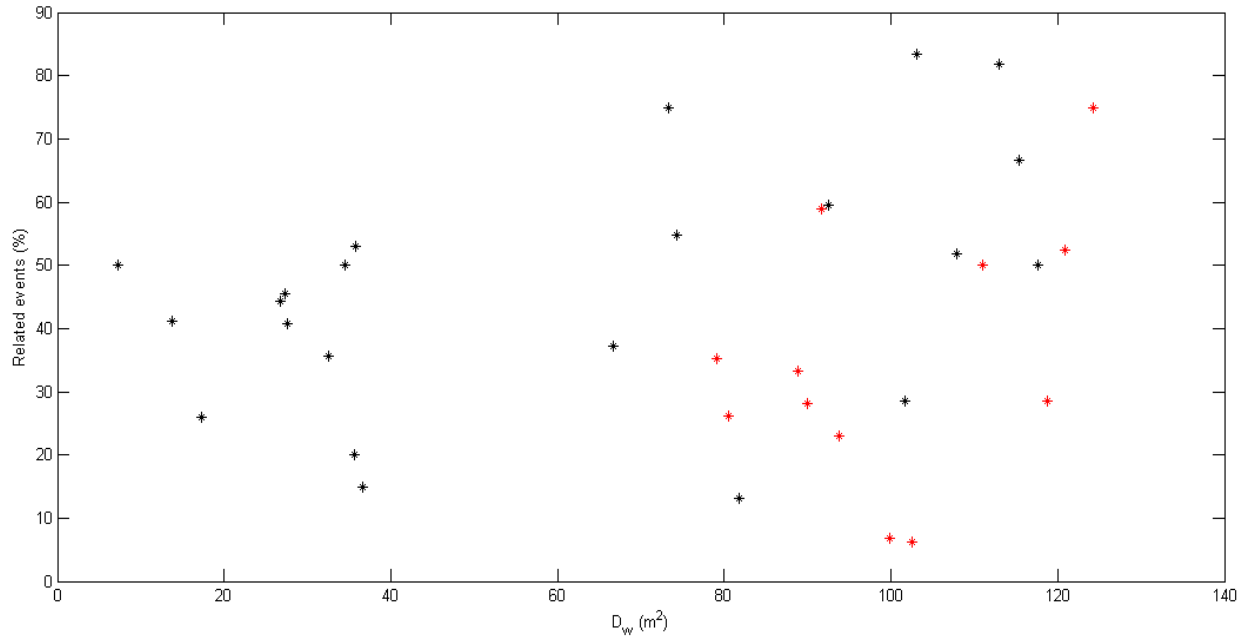

Figure 37: Relation between the percentage of TKE events which can be related to a SSC event and the short-wave dissipation. Conditions near the edge of the surfzone are coloured red ($\zeta \approx 1$). Threshold value $\mu + 4\sigma$ and window size $1T_p$.

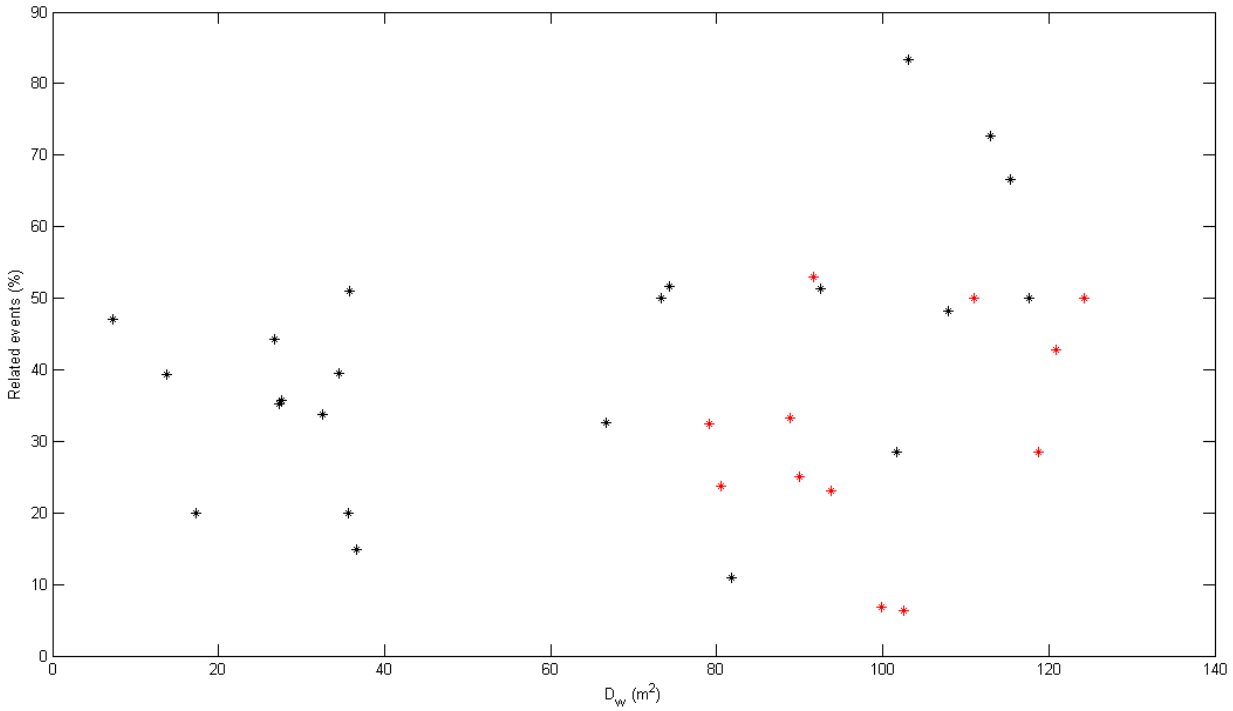

Figure 38: Relation between the percentage of TKE events which can be related to a SSC event and the short-wave dissipation. Conditions near the edge of the surfzone are coloured red ($\zeta \approx 1$). Threshold value $\mu + 4\sigma$ and window size $0.75\ T_p$.

9. Conclusions

This thesis was written to investigate the influence of breaking-induced turbulence on sediment entrainment in the surfzone. TKE and SSC patterns were observed at different cross-shore positions and it was tried to find a relationship between TKE and SSC events.
The turbulent kinetic energy is related to the cross-shore position. At the edge of the surfzone, turbulence intensities can reach high values (up to $\sqrt{\overline{k}/gh} \approx 0.08$), whereas at other locations the turbulence intensity is limited. From this it can be concluded that breaking waves can induce large turbulence intensities ($\sqrt{\overline{k}/gh} > 0.025$).
The vertical structure of the turbulent kinetic energy in the water column differs depending on the cross-shore position. Outside the location of the surfzone edge, the near-bed ($z/h \approx 0.1$) $\sqrt{\overline{k}/gh}$ is much larger than both the centred ($z/h = 0.2 - 0.3$) and top ($z/h = 0.4 - 0.5$) $\sqrt{\overline{k}/gh}$. The centred and top $\sqrt{\overline{k}/gh}$ are approximately equal. During intense turbulent conditions, located near the edge of the surfzone, usually both the near-bed ($z/h \approx 0.15$) and centred ($z/h > 0.3$) $\sqrt{\overline{k}/gh}$ are smaller than the top ($z/h > 0.5$) $\sqrt{\overline{k}/gh}$. From this it can be concluded that the prevailing source for turbulence under breaking waves is the water surface and thus breaking-induced turbulence. The turbulence source under non-breaking waves is the bottom boundary layer.

Similar to the turbulent kinetic energy, suspended sediment concentrations are related to cross-shore position. Around the edge of the surfzone, mean sediment concentrations at z= 0.040 m and z = 0.035 m can reach 6.5 kg/m^3. Seaward of the surfzone, mean sediment concentrations are smaller and reach concentrations of up to 3.5 kg/m^3 at the same elevation above the bed. Since the largest waves break and plunging breakers are dominant over bores near the edge of the surfzone, intense turbulent conditions are generated in here. Therefore it can be concluded that breaking waves cause larger suspension concentrations compared to non-breaking waves. Up in the water column sediment concentrations can still be high of about 3 kg/m^3. The suspended-sediment concentrations gradient in the upper water column is more or less 0. From this it is concluded that breaking waves also cause a strong vertical mixing of sediment in the water column.

The mean turbulent kinetic energy and mean suspended-sediment concentrations near the bed are related to each other, since increasing near-bed turbulence created larger near-bed sediment concentrations. Nonetheless the number of SSC events did not depend on the number of TKE events, because the number of SSC events is not solely determined by local processes, but also non-local processes such as advection. The percentage of TKE events

which can be related to SSC events has no clear relation with the short-wave dissipation and is dependent on the threshold value used to determine the events. A threshold value of $\mu + 4\sigma$ shows a better relation for conditions near the edge of the surfzone compared to the threshold value $\mu + 3\sigma$.

References

Aagaard, T. and Hughes, M.G., 2010. Breaker turbulence and sediment suspension in the surf zone. *Marine Geology*, **271**, 250-259.

Baldock, T.E., Holmes, P., Bunker, S. and Van Weert, P., 2004. Cross-shore hydrodynamics within an unsaturated surfzone. *Coastal Engineering*. **34**, 173-196.

Beach, R.A. and Sternberg, R.W., 1996. Suspended-sediment transport in the surf zone: response to breaking waves. *Continental Shelf Research*, **16** (No. 15), 1989-2003.

Butt, T., Russell, P., Puleo, J., Miles, J. and Masselink, G., 2004. The influence of bore turbulence on sediment transport in the swash and inner surf zones. *Continental Shelf Research*, **24**, 757-771.

Cox, D.T. and Kobayashi, N., 2000. Identification of intense, intermittent coherent motions under shoaling and breaking waves. *Journal of Geophysical Research*, **105**, 223-236.

Feddersen, F. and Williams, A.J., 2007. Direct estimation of the Reynolds stress vertical structure in the nearshore. *Journal of atmospheric and oceanic technology*. **24**, 102-116.

Feddersen, F., 2012. Observations of the surfzone turbulent dissipation rate. *American Meteorological Society*, **42**, 386-399. doi: 10.1175/JPO-D-11-082.1

Govender, K., Mocke, G.P. and Alport, M.J., 2004. Dissipation of isotropic turbulence and length-scale measurements through the wave roller in laboratory spilling waves. *Journal of Geophysical Research*, **109**, C08018, doi: 10-1029/2003JC002233.

Grasso, F. and Ruessink, B.G., 2011. Vertical structure of the turbulence dissipation rate in the surf zone. *Journal of Coastal Research*. SI **64** (Proceedings of the 11th International Coastal Symposium), 90-94.

Jaffe, B. and Sallenger, A., 1992. The contribution of suspension events to sediment transport in the surf zone. *Coastal Engineering 1992*, chapter 205, 2680-2693.

Kana, T.W., 1979. Suspended sediment in breaking waves. *(Coastal Res. Div. Tech. Rep. No. 18)*, Dept. of Geology, University of South Carolina, Columbia, SC, 153 pp.

Mori, N., Ueno, S. and Kakuno, S., 2007. Noise of acoustic Doppler velocimeter data in bubbly flows. *Journal of Engineering Mechanics*. **133**, 122-125.

Nadoaka, K., 1986. A fundamental study on shoaling and velocity field structure of water waves in the nearshore zone. Tech. Rept. Of Dept. Civil Engineering, Tokyo Institute of Technology, **36**, 33-125.

Nadoaka, K., Ueno, S. and Igarashi, T., 1988. Sediment suspension due to large scale eddies in the surf zone. Dept. Civil Eng., Tokyo Institute of Technology O-okayama 2-12-1, Meguro-ku, Tokyo 152, Japan.

Ogston, A.S. and Sternberg, R.W., 2002. Effect of wave breaking on sediment eddy diffusivity, suspended-sediment and longshore sediment flux profiles in the surfzone. *Continental Shelf Research*, **22**, 633-655.

Roelvink, J.A. and Stive, M.J.F., 1989. Bar-generating cross-shore flow mechanisms on a beach. *Journal of Geophysical Research*, **94**, 4785-4800.

Ruessink, B.G., 2010. Observations of turbulence within a natural surf zone. *Journal of Physical Oceanography*, **40**, 2696-2712.

Schlax, M.G. and Chelton, D.B., 1992. Frequency domain diagnostics for linear smoothers. *Journal of the American Statistical Association*. **87**, 1070-1081.

Scott, C.P., Cox., D.T., Maddux, T.B. and Long, J.W., 2005. Large-scale laboratory observations of turbulence on a fixed barred beach. *Measurement Science and Technology*. **16**, 1903-1912. doi: 10.1088/0957-0233/16/10/004

Scott, N.V., Hsu, T-.,J. and Cox, D., 2009. Steep wave, turbulence, and sediment concentration statistics beneath a breaking wave field and their implications for sediment transport. *Continental Shelf Research*, **29**, 2303-2317. doi:10.1016/j.csr.2009.09.008

Svendsen, I.A., 1984. Mass flux and undertow in the surf zone. *Coastal Engineering*, **8**, 347-365.

Trowbridge, J.H., 1998. On a technique for measurement of turbulent shear stress in the presence of surface waves. *Journal of atmospheric and oceanic technology*. **15**, 290-298.

Yoon, H.D. and Cox, D.T., 2009. Large-scale laboratory observation of wave breaking turbulence over an evolving beach. *Journal of Geophysical Research*, **115**, C10007, doi:10.1029JC005748.

Yu, Y., Sternberg, R.W. and Beach, R.A., 1993. Kinematics of breaking waves and associated suspended sediment in the nearshore zone. *Continental Shelf Research*, **13**, 1219-1242.